DEVELOPMENT OF A MULTI-CHANNEL HANDHELD PROBE DESIGNED FOR NEAR INFRARED SPECTROSCOPY AND AN EXPLORATION INTO ITS CLINICAL APPLICATIONS

by

PRADHEEP RAMAN

Presented to the Faculty of the Graduate School of

The University of Texas at Arlington in Partial Fulfillment

of the Requirements

for the Degree of

MASTER OF SCIENCE IN BIOMEDICAL ENGINEERING

THE UNIVERSITY OF TEXAS AT ARLINGTON

May 2006

ACKNOWLEDGEMENTS

I take this opportunity to express my deepest gratitude to all the people who helped me through the course of my thesis.

The first person I would like to express my sincere thanks is my mentor Dr. Hanli Liu. I have known her as a sincere, hardworking professional with high enthusiasm on research. She has been a guiding light throughout my research career. I have great pleasure that I came to know such a wonderful person. Moreover, I am extremely honored to have worked under her.

I would also like to express my sincere gratitude and thank to Dr. Anna Ratka for accepting to be a committee member and also for helping me with all the invaluable suggestions and support that was required to complete this project.

I would also like to express my thanks to Dr. Khosrow Behbehani for accepting to be a committee member and also for his invaluable time.

I would like to thank all my lab members and my friends for their invaluable suggestions and cooperation from time to time during the project.

Especially, I would like to thank my parents who have been a constant source of support and inspiration at all times. It is because of their sacrifice, love and encouragement that I have been able to achieve my goal until today.

December 9, 2005

ABSTRACT

DEVELOPMENT OF A MULTI-CHANNEL HANDHELD PROBE DESIGNED FOR NEAR INFRARED SPECTROSCOPY AND AN EXPLORATION INTO ITS CLINICAL APPLICATIONS

Publication No. _____

Pradheep Raman, M.S.

The University of Texas at Arlington

and

The University of Texas Southwestern Medical Center at Dallas, 2006

Supervising Professor: Dr. Hanli Liu

Near Infrared (NIR) spectroscopy and imaging has become popular in research fields for the past 2 decades. My research focuses on the development of a handheld, multi-channel, multi-separation probe for the low-cost, compact, NIR spectroscopy (LCC-NIRS) system and also on the exploration into its possible clinical applications. The work is divided into three parts. The first part deals with the development of the multi-separation probe with source-detector separation of 3.8 cm, 3.3 cm, 3.0 cm, and 2.3 cm. The probe is designed to work as a tri-wavelength system for the LCC-NIRS, which was developed earlier, consisting of one light emitting diode (LED) as the source and four photo detectors. The source is a tri-wavelength LED, emitting light at 730 nm, 805

nm, and 850 nm. The physiological data was acquired from four, multi-separation channels, while the LED light switched between the three wavelengths. The probe holder was designed to the specifications of the multi-separation probe as discussed earlier. It was made using VeriSiTal (VST) silicone elastomers, a new concept in silicone technology. A laboratory phantom experiment was done to validate the new probe's functionality with the LCC–NIRS system to detect Hb (deoxygenated hemoglobin) and HbO2 (oxygenated hemoglobin) changes occurring inside the tissue phantom. The phantom was made with a static blood phantom using horse blood mixed with intralipid solutions.

In the second part, the LCC-NIRS system's possible clinical application, i.e., as a screening tool for the detection of sleep apnea, was explored using the breath holding protocol. In persons with obstructive sleep apnea, there is a reduction in their oxy-hemoglobin saturation (O_2 saturation), due to the cessation of airflow, resulting from the progressive collapse of the upper airway. This is simulated using the breath holding protocol. The results obtained proved that the LCC-NIRS system was able to detect the hemodynamic changes during the protocol used.

In the third part, LCC-NIRS system was employed to measure hot flashes, one of the most common and troublesome symptoms of menopause. The studies proved very fruitful as the system was able to detect changes in local blood volume during hot flash events.

Further development can be done to add many features to this LCC-NIRS system so as to make it more compact and eventually a wireless system, which can be very helpful for other clinical uses.

TABLE OF CONTENTS

LIST OF ILLUSTRATIONS

LIST OF TABLES

CHAPTER 1

INTRODUCTION

1.1 Near Infrared Spectroscopy (NIRS)

1.1.1 Background

Infrared light is a part of the electromagnetic spectrum lying between the visible range and the microwave range. Infrared light can also be broken down into "Near Infrared" light, "Mid Infrared" light, and "Far Infrared" light [1, 2], as shown in Fig. 1.

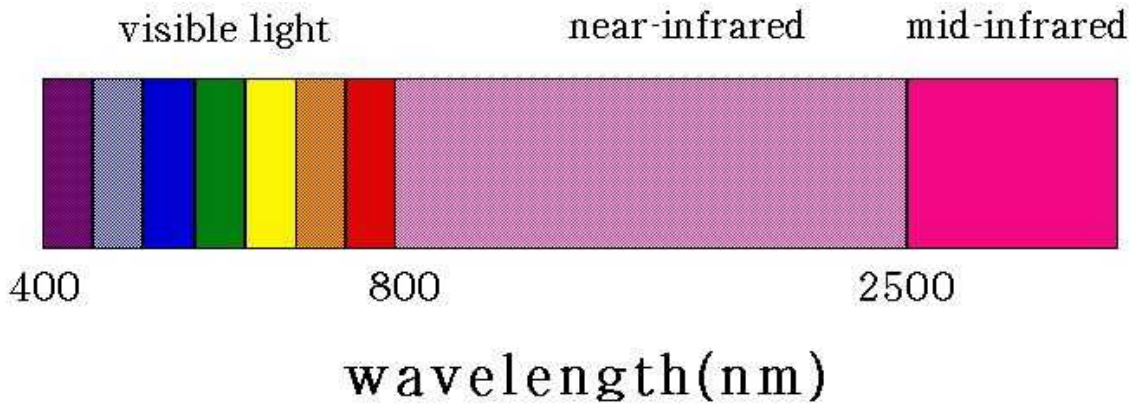

Figure 1.1 Optical portion of the electromagnetic spectrum [3]

The use of near infrared (NIR) light for spectroscopy and imaging is based on the different wavelength dependent absorption and scattering properties of tissues. The wavelengths used typically vary from 650 to 1000 nm, a range of wavelengths often referred to as the "optical window of body tissues". At these wavelengths, many tissues are relatively transparent to light [4].

1.1.2 Tissue Optical Properties

The principal idea in near infrared spectroscopy and imaging is to measure the properties of reflected light on the surface of the tissue at some distance apart from the light source. In spectroscopic applications the concentrations of absorbing molecules such as oxyhemoglobin (HbO2) and de-oxyhemoglobin (Hb) can be estimated [4]. As it is well known that the transmission and absorption of light in human body tissues are sensitive to its hemoglobin concentration, the better penetrating near infrared light, rather than visible light, is used to measure changes in blood hemoglobin concentrations in the body tissues. The high sensitivity of near infrared tissue spectroscopy to changes in hemoglobin concentration affords the detection of small optical signals from biological tissues such as the cerebral hemodynamic fluctuations [5].

The light propagation inside a tissue is mainly governed by two physical phenomena, i.e., light absorption and scattering. Within the human tissue, there exist substances which absorb light. The absorption spectra, for these substances, within the NIR wavelengths are well defined. The absorbing particles within the tissue can be grouped into two categories: one whose concentration changes with time and the other whose concentration remains constant with time. The concentration of absorbers such as water, melanin, and bilirubin remain constant with time. But concentrations of other absorbers like oxyhemoglobin (Hb) and de-oxyhemoglobin (HbO2) are strongly affected by the tissue oxygenation and metabolism. At NIR wavelengths, by measuring the Hb and HbO_2 concentrations, useful physiological information can be extracted [6, 7].

Figure 1.2 shows absorption spectra of water, and Figure 1.3 shows the extinction coefficients spectra of Hb and HbO2 [6]. As can be seen from these three figures, absorption due to water dominates at wavelengths above 1000 nm, and, below 650 nm is dominated by absorption due to hemoglobin (Hb and HbO2).

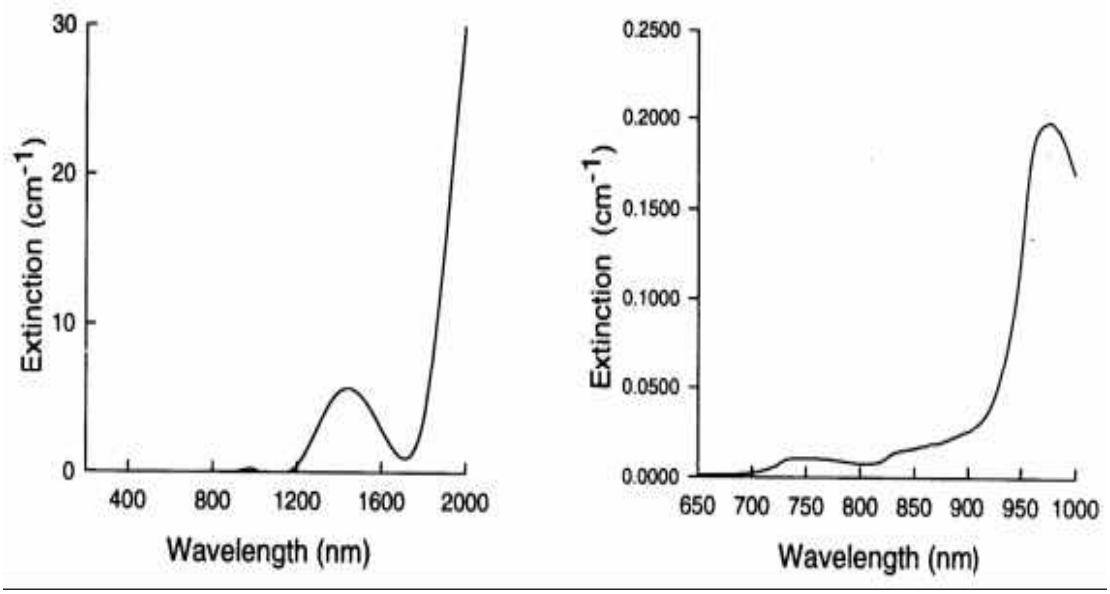

Figure 1.2 Absorption spectra of pure water [6]

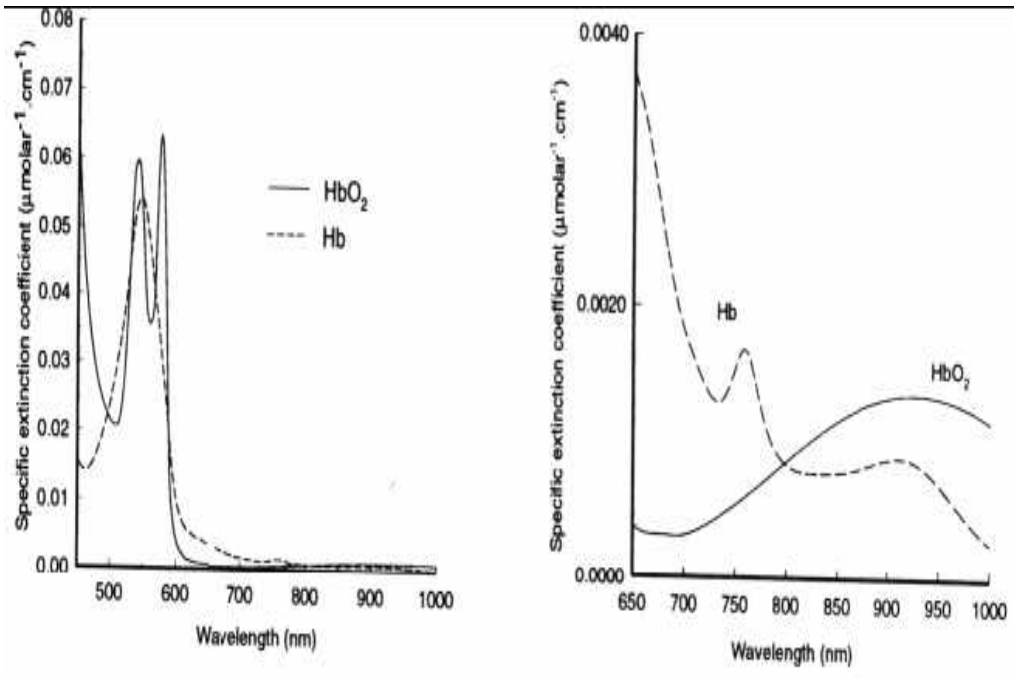

Figure 1.3 Absorption spectra for Hb and HbO_2 [6]

As seen from Figure 1.3, the main absorbers, within the 650 nm – 950 nm wavelengths called the 'near infrared window' or 'optical window of tissues', are Hb and HbO2.

1.2 Types of Instruments for NIRS

The methods used for near-infrared imaging can be divided into three classes: time resolved, frequency resolved and continuous wave techniques. The basic principle of measurement for all three techniques remains the same: i.e., the NIR light is delivered on the surface of the tissue by a source. At the measurement site, typically a few centimeters apart from the source position, the NIR light is collected by the detector [4].

Time Resolved Systems:

In the time-domain techniques, a short laser pulse is used as the input, and the distribution of the time-of-flights of the photons is measured. The detectors receive the temporal distribution of photons as they leave the tissue; this temporal distribution is called the 'temporal point spread function' (TPSF), from which data such as mean time of flight can be retrieved. The time-domain system permits quantification of absolute values for absorption coefficient (μ_a) and reduced scattering coefficient (μ_s'), when a complete TPSF is recorded at the detector at a fixed source detector separation [4]. Figure 1.4(a) shows the TPSF after an impulse passes through the tissue [10]. However, these systems suffer from the drawback that they are very slow and expensive, though they provide the maximum information per source detector pair [8].

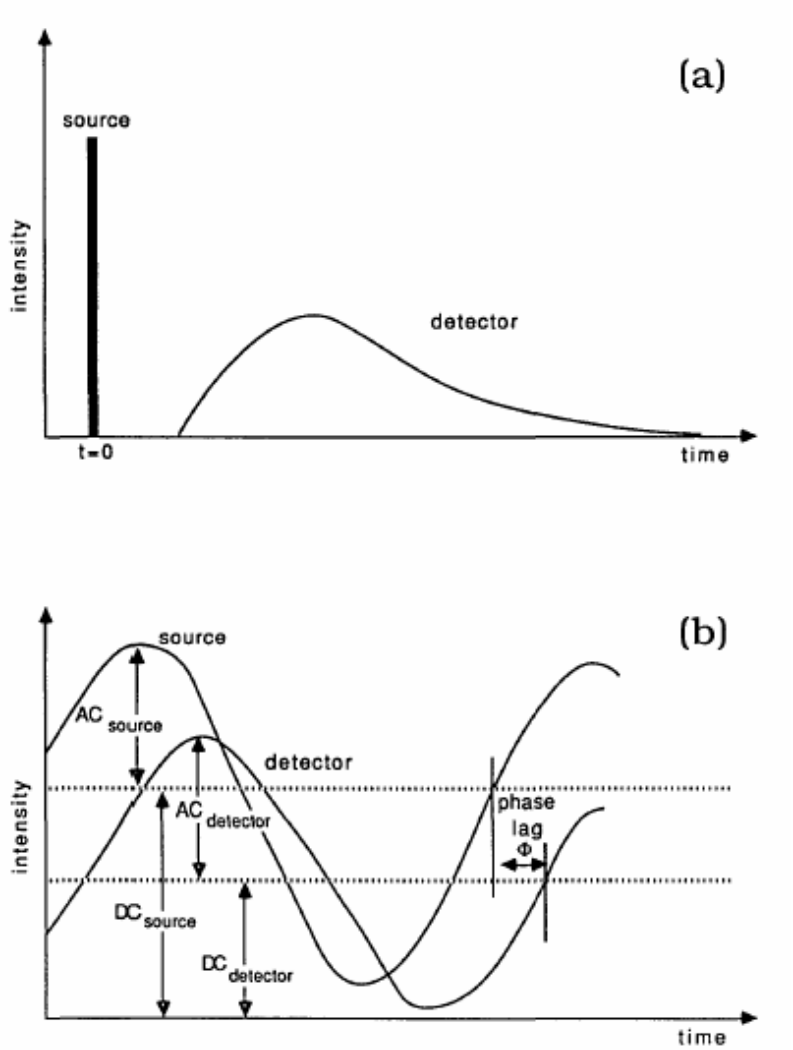

Figure 1.4 An illustration of the working principles of a) the time-domain and b) the frequency-domain NIRS instruments [10]

Frequency Domain Systems:

Frequency domain systems use a light source whose intensity is modulated at frequencies of tens to hundreds of megahertz (typically between 50 to 800 MHz). This gives rise to a photon density wave propagating in the tissue. At the detector side, by measuring the amplitude change and the phase shift relative to the amplitude and the phase of the source light, absolute values for absorption and scattering coefficients can be

estimated[7, 8]. Figure 1.4(b) shows the principle of this system [10]. An example of this kind of system is the ISS Oximeter used by many researchers in this field.

Continuous Wave Systems:

Continuous Wave (CW) systems use a source which emits continuous light at constant amplitude. The detectors collect the light coming out from the tissues. By taking measurements at two wavelengths, a relative change in the Hb and HbO2 concentrations can be calculated.

CW systems are comparatively easy to build and acquire data quickly. The major drawback of these systems is that they do not provide absolute values of Hb or HbO2 concentrations within the tissue, which the frequency domain and time domain systems are able to provide information about.

1.2.1 Theory of Continuous Wave Measurement

In a purely absorbing medium, the propagation of light through the medium obeys Beer-Lambert's law. The law states that the attenuation (*OD*) is proportional to the concentration of the absorbing compound in the solution (*c*) and the optical pathlength (*d*):

$$OD = \log_{10} [I_0/I] = \varepsilon.c.d. \qquad (1.1)$$

where, OD is the attenuation measured in optical densities, I_0 is the intensity of the incident light, I is the intensity of the transmitted light, ε ($mMol^{-1}$ cm^{-1}) is the specific extinction coefficient of the absorber, c (mMol) is the concentration of absorbing

compound in solution, d is the distance of separation between the source and the detector.

For a medium having multiple absorbing compounds, the overall attenuation is the linear sum of individual contributions as given by equation 1.2.

$$OD = \log_{10} [I_0/I] = [\varepsilon_1.c_1 + \varepsilon_2.c_2 + \ldots. + \varepsilon_n.c_n].d. \quad (1.2)$$

However, in human tissues there exists another phenomenon, other than absorption, which contributes to attenuation. The other dominant phenomenon is called light scattering. It modifies the path taken by the light within the tissue, thereby altering the optical path length. Therefore, the Beer Lambert's law was modified as the absorption changes were difficult to quantify due to light scattering. The modified Beer Lambert's Law is given by:

$$OD = \log_{10} [I_o/I] = \varepsilon.c.d.\ DPF + G, \quad (1.3)$$

where G is the term added to compensate for scattering losses, and DPF is the differential path length factor. The modified Beer Lambert law can also be written as:

$$OD = \log_{10} [I_o/I] = \mu_a.L + G, \quad (1.4)$$

where $\mu_a = \varepsilon.c$ is the absorption coefficient, and L = d.DPF is the optical path length.

For relative measurements as done with the CW systems, a change in attenuation from the baseline condition to transient condition at wavelength λ is calculated as:

$$\Delta OD^{\lambda} = OD^{\lambda}\,(\text{transient}) - OD^{\lambda}\,(\text{baseline})$$

$$= \log_{10} (I_b/I_t)^{\lambda} = \Delta \mu_a{}^{\lambda}.L^{\lambda} \quad (1.5)$$

The major assumption here is that the path length is a constant for all wavelengths [9]. Therefore, L^{λ} remains a constant for all the wavelengths. Since the two main

chromophores in tissue for the NIR window are Hb and HbO_2, changes in absorption coefficients at two wavelengths can be given by:

$$\Delta\mu_a^{\lambda 1} = (\varepsilon_{Hb}^{\lambda 1}Hb + \varepsilon_{HbO2}^{\lambda 1}HbO2)_t - (\varepsilon_{Hb}^{\lambda 2}Hb + \varepsilon_{HbO2}^{\lambda 2}HbO2)_{b,} \quad (1.6)$$

$$\Delta\mu_a^{\lambda 2} = (\varepsilon_{Hb}^{\lambda 2}Hb + \varepsilon_{HbO2}^{\lambda 2}HbO2)_t - (\varepsilon_{Hb}^{\lambda 2}Hb + \varepsilon_{HbO2}^{\lambda 2}HbO2)_{b.} \quad (1.7)$$

So, $\Delta\mu_a^{\lambda}$ can be written as,

$$\Delta\mu_a^{\lambda} = \varepsilon_{Hb}^{\lambda}.\,\Delta[Hb] + \varepsilon_{HbO2}^{\lambda}.\Delta[HbO2]$$

$$= \log_{10}(I_b/I_t)^{\lambda}/\,L^{\lambda} \quad (1.8)$$

It follows that $\Delta\mu_a$ values at two different wavelengths are given by equations 1.9 and 1.10,

$$\Delta\mu_a^{\lambda 1} = \varepsilon_{Hb}^{\lambda 1}.\,\Delta[Hb] + \varepsilon_{HbO2}^{\lambda 1}.\Delta[HbO2], \quad (1.9)$$

$$\Delta\mu_a^{\lambda 2} = \varepsilon_{Hb}^{\lambda 2}.\,\Delta[Hb] + \varepsilon_{HbO2}^{\lambda 2}.\Delta[HbO2]. \quad (1.10)$$

Now, we have two simultaneous equations and two unknowns. By solving for these two equations, it is possible to obtain $\Delta[Hb]$ and $\Delta[HbO2]$ as given by equations 1.11 and 1.12:.

$$\Delta H\ b = \frac{\Delta\mu_a^{\lambda_2} - \varepsilon_{H\ b}^{\lambda_1}\ a\ \Delta\mu_{H\ 2b}^{\lambda_1}\varepsilon_{O}^{\lambda_2}}{\varepsilon_{H\ b2}^{\lambda_1}\varepsilon_{O\ H\ b}^{\lambda_2} - \varepsilon_{H\ b}^{\lambda_2}\varepsilon_{2H\ b\ O}^{\lambda_1}} \quad (1.11)$$

$$\Delta H\ b = \frac{\Delta\mu_a^{\lambda_1} - \varepsilon_{H\ b}^{\lambda_2}\ a\ \Delta\mu_{H\ b}^{\lambda_2}\varepsilon_{b}^{\lambda_1}}{\varepsilon_{H\ b2}^{\lambda_1}\varepsilon_{O\ H\ b}^{\lambda_2} - \varepsilon_{H\ b}^{\lambda_2}\varepsilon_{2H\ b\ O}^{\lambda_1}} \quad (1.12)$$

The total ($\Delta[Hbt]$) is calculated as

$$\Delta[Hb_t] = \Delta[Hb] + \Delta[HbO2] \quad (1.13)$$

Δ[Hbt] is directly proportional to blood volume [11]. Blood volume within the tissue is given by the relation [11],

$$\Delta BV_t = \frac{V * M}{K} [\, b \,] \qquad (1.14)$$

where, ΔBV_t is the blood volume within the tissue under interrogation in liters, K is the hemoglobin concentration in gram/liter for liquid blood, V is the tissue volume in cm^3, M is the hemoglobin molecular weight in grams/mole.

1.3 Research Outline

The focus of my study was to develop a multi-separation, multi-channel, and handheld probe for the LCC – NIRS system to be described in Chapter 2. This thesis consisted of five parts: firstly, the development of the above mentioned probe is described in detail in Chapter 2. Chapter 3 deals with the testing of this probe with a static blood phantom model. Then two possible applications of this Low Cost and Compact (LCC) Continuous Wave (CW) Near Infrared Spectroscopic (NIRS) system are explored in Chapters 4 and 5. Chapter 4 deals with the preliminary study to test the capability of LCC-NIRS system as a screening tool to detect Sleep Apnea. Another possible application explored is to utilize the LCC-NIRS system for detection of hot flashes in post menopausal women. The results supporting this idea and the details of this study will be reported in Chapter 5.

CHAPTER 2

LABORATORY BASED NEAR INFRARED SPECTROSCOPIC SYSTEM

In previous studies on cerebral hemodynamic changes and hot flash measurement, a commercial system (LEDI), manufactured by NIM (Near Infrared Monitor) Inc. (Philadelphia, PA) [14], was used [15]. The main drawback of this system was its probe design. The probe was made for measurement from the forehead only, which limits the system's capability to measure other physiological phenomena from other sites on the body. Thus, a Low Cost and Compact (LCC) NIRS system was built by a former BME graduate student in our lab [15].

As part of my thesis, I developed a new, compact, multi-channel, and multi-source-detector separation probe for the system mentioned above as explained in the following sections of this chapter. Two possible clinical applications, for which the system could be used, are also explored as part of my thesis and will be reported in the following chapters.

2.1 Low Cost & Compact (LCC) NIRS System

The Hardware of the LCC-NIRS system was developed earlier by V. Sharma [15] and consists of three components: 1) a control circuitry which helps in the switching of the Light Emitting Diodes (LED) and the adjustment of the gain for the detectors, 2) a dual variable power supply which supplies ± 5V for the detectors and 8V for the LED, and 3) an NIDAQ card 6036-E used for data acquisition and triggering of the LED

control circuit. Another important component for the system is a multi-channel, multi-separation probe which has one light source and four detectors. Making such a probe is one of my major contributions to the project, and I will describe it in further detail in the later part of this chapter. The block diagram and the picture of the whole system are shown in Figs. 2.1 and 2.2.

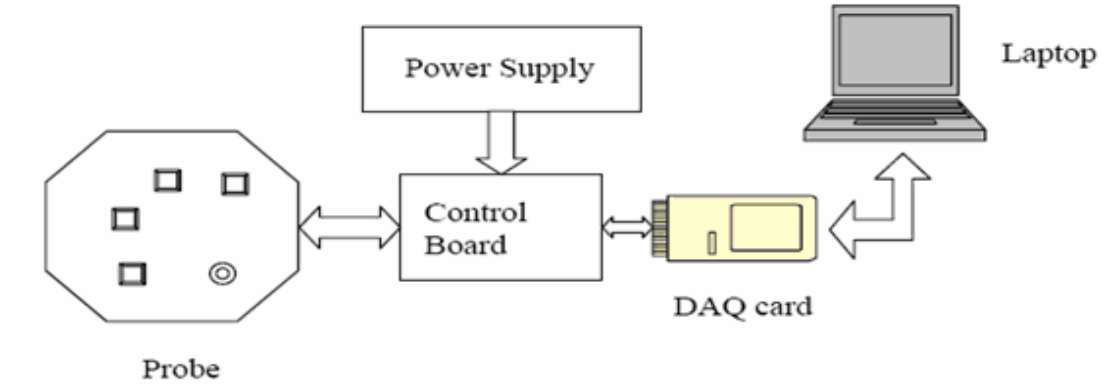

Figure 2.1 Block diagram of the LCC-NIRS system.

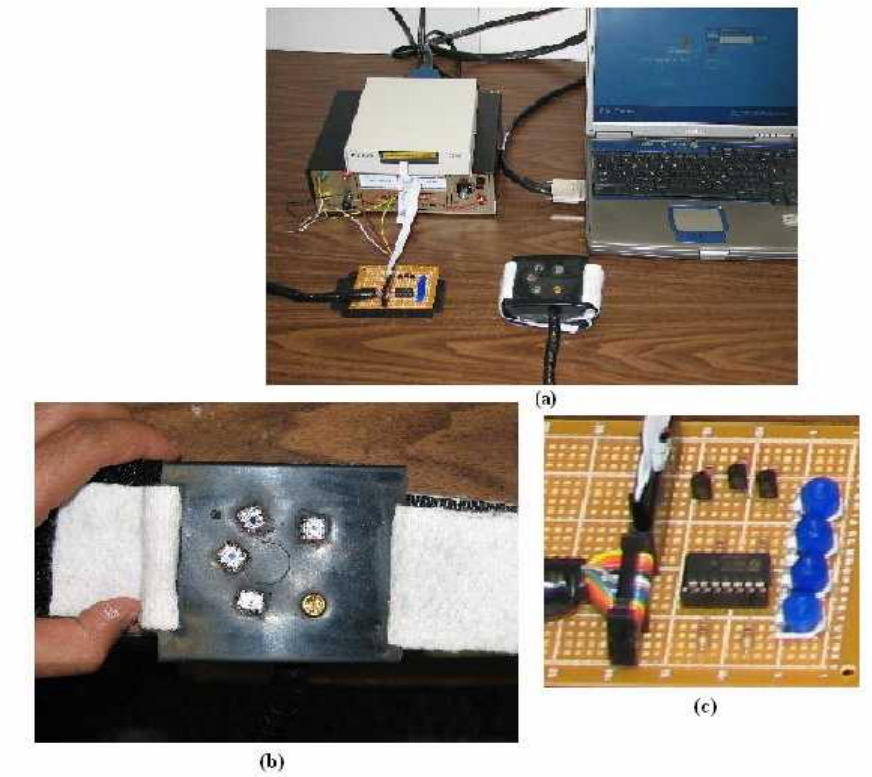

Figure 2.2 A picture of (a) the entire LCC-NIRS system, closer look at (b) the multi-channel, multi-separation probe, and (c) the control board.

The detailed information on the hardware design, circuit implementation and computer interface for the LCC-NIRS device can be found in Ref. 15. A brief summary on the hardware is given below.

Control Board: The functions of control board include amplification of the pre-amplified signals from the photo detectors and the switching of the LED between the three wavelengths (730 nm, 805 nm, and 850 nm) [15].

Power Supply: The power supply provides a biasing voltage of ±5V to each of the transistors used for switching among the three wavelengths. The power supply also

provides an 8V bias to the anode of each LED, while the cathode of each LED is connected to the collector of the transistor [15].

DAQ Card: The data acquisition from the photo diodes and the LED switching control is done via the NI DAQ card 6036-E. The DAQ card is controlled using a software code written in LABVIEW. The dynamic range of the DAQ card is 16-bit with a resolution of $1/2^{16}$ [15].

Interface Software: LABVIEW 7.1, developed by National Instruments Inc., was used to program the DAQ card in order to acquire data from the four channels and also to control the switching of the LED source from on to off positions .The LED is turned on at a wavelength of 730 nm. 50 data points is acquired from each detector at the rate of 50 kHz. 50 data points are then averaged to get 4 data points from the four channels. Then the LED is turned off. The same procedure is repeated for the other two (805 nm and 850 nm) wavelengths. The 12 data points (4 channels X 3 wavelengths) are stored into an array, which forms a data set. Data is acquired at a rate of 5 Hz, i.e. one data set (12 data points) is acquired every 200 ms, but this frequency can be changed from the front panel [15].

The data was analyzed with a program written in MATLAB as shown in Appendix A. As the LABVIEW program does not allow putting markers during the experiment, the marker locations (in seconds) need to be noted before running the calculation program.

2.2 Probe Development

The probe is designed to work with one LED, which acts as the source, and four photo detectors. The source is a tri-wavelength LED, emitting light at 730 nm, 805 nm, and 850 nm. Hb and HbO2 can be calculated, using the equations described in the previous chapter, from the detected signals at 730 nm and 850 nm. Therefore, the measurement at these wavelengths yields a direct approximation of the blood volume changes [15]. The physiological data was acquired from four, multi-separation channels, while the LED light switched between the three wavelengths.

2.2.1 Probe Design

The probe consists of a tri-wavelength LED in one corner, as the source, and four photo detectors. The source LED (L4*730/4*805/4*850-40Q96-I Epitex Inc.) emits light at three wavelengths (730 nm, 805 nm, 850 nm). The detectors used are OPT101, manufactured by Burr-Brown [15], and they are at different distances from the source LED and placed around the source. The multi-distance between the source and detectors is of particular significance, as it provides information regarding the depth of penetration of light within the tissue as explained in Chapter 3. The approximate source detector separations are 2.3 cm, 3.0 cm, 3.3 cm and 3.8 cm respectively. The distances were measured between the centers of the source LED and the photo diodes respectively.

2.2.2 Probe Holder Design

The probe holder was designed to the specifications of the multi-separation probe as discussed earlier. It was made from VeriSiTal (VST) silicone elastomers, a new concept in silicone technology. This elastomer is produced by Factor II Inc. The VST line of elastomers is a translucent two-component (10:1 mixing by weight), low viscosity, addition cure (platinum) Room Temperature Vulcanizing (RTV) silicone elastomer. This material is available in various forms. The type that has been used here is VST – 50 as shown in Figure 2.3. The VST – 50 is a two-component elastomer, consisting of a Base (Part A) and a Catalyst (Part B) with a cure RTV time of 24 hours [18].

Figure 2.3 VST – 50 Silicone Elastomer [17]

The moulds, as shown in Figure 2.4, for the detectors were made from hard thermacol with the dimensions shown in Figure 2.5. The moulds were fixed onto a plastic

transparent container at the desired distances (2.3 cm, 3.0 cm, 3.3 cm, 3.8 cm) from the source location and marked on the outside of the container using a permanent marker.

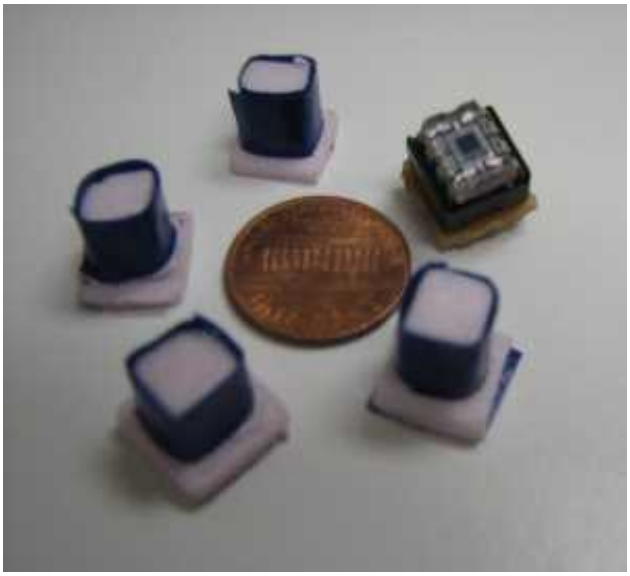

Figure 2.4 Picture of the detector moulds along with an actual detector

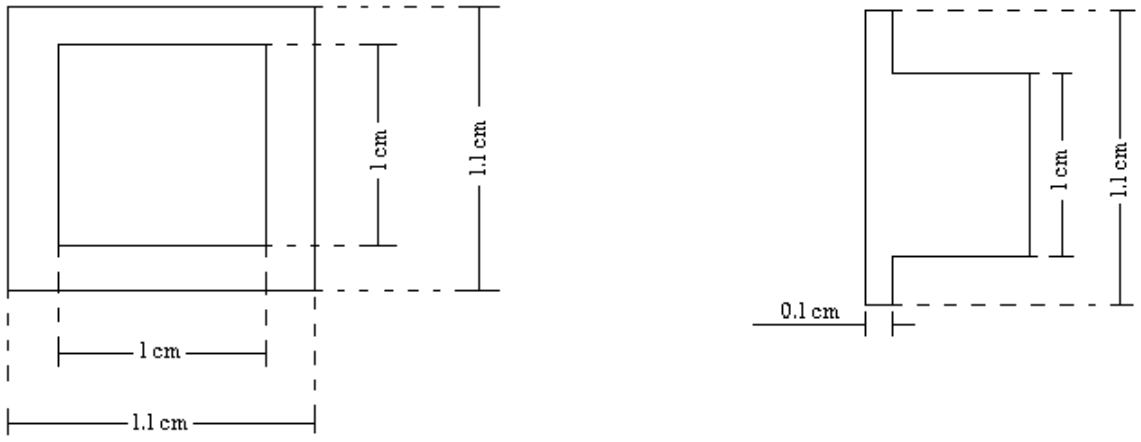

Figure 2.5 Top view and Side view of the detector moulds

Figure 2.6 Picture of the top and side views of the detector moulds with the model of an actual detector

Then about 200 grams of the Base (Part A) were weighed on a weighing scale after the Base was well stirred before it was taken into a clean container. The Catalyst (Part B) was well shaken before adding about 20 grams of the catalyst to the Base in the clean container. Thus the ratio for the Base: Catalyst was maintained to be 10:1. Black ink was added to the mixture to get the desired black color for the probe holder. Then the mixture was well stirred with a spatula until it reached a uniform black color. The container walls and bottom was well scraped during the stirring process. Next, the mixture was poured into the transparent plastic container until the detector moulds were completely covered by it. Care was taken while pouring the mixture into the mould to minimize the trapping of air bubbles. The mixture was allowed to cure for 24 hours [18].

After 24 hours, the silicone elastomer gained maximum strength. Then, the moulds could be removed from the elastomer. The source location was determined and a

hole was punched, where the source LED was inserted. At the detector locations, slits were made from the back to insert the detectors (photo diodes) into the correct locations.

Two long slits were further made along the length of the two sides of the probe (see Figure 2.7). Then a velcro band of the desired size was cut, and the sticky side of the band was taped with a first aid tape. The Velcro belt was inserted into the two slits, so that it came from both ends to form a strap around the probe holder. A thin transparent film is then placed on the detector side of the probe, so as to reduce the variation of distances between the detector and the body tissue. The final design of the probe is as shown in Figure 2.7 below.

Figure 2.7 Final design of the multi-channel probe

CHAPTER 3

MULTI-DISTANCE SEPARATION INVESTIGATION

This chapter deals with the propagation of light inside the biological tissue. Light scattering occurs at borders of media with different refractive indices. The photons diffuse into the tissue up to depths of about a few centimeters providing the averaged absorption and scattering properties of the tissue. The human tissue is relatively transparent to light in the NIR wavelength range, as the absorption due to water and hemoglobin is minimal.

3.1 Light Travel in Human Tissues (Banana Concept)

Photon migration through biological tissue can be well described by diffusion theory. The photon fluence density function $\phi(r, t)$, expressed in number of photons per unit area per unit time, satisfies the equation,

$$\frac{1}{c}\frac{\partial \phi(r, t)}{\partial t} - D\nabla^2\phi(r, t) + \mu_a\phi(r, t) = S(r, t), \qquad (3.1)$$

where μ_a is the absorption coefficient measured in the unit of inverse length, $D = 1/3[\mu_a + (1-g)\mu_s]$ is the diffusion coefficient measured in the unit of a length scale, and c is the speed of light traveling inside the diffusive medium with a refractive index of n.. Here, $g = \langle \cos\theta \rangle$ (θ is the scattering angle), and μ_s is the scattering coefficient also measured in the unit of inverse length. In the NIR wavelength range, as discussed in Chapter 1, the absorption due to hemoglobin and water is relatively small. Therefore, the reduced scattering coefficient is given as $\mu_s' = (1-g)\mu_s$, which describes the isotropic diffusion

processes at large distances. The speed of light traveling inside tissue is given by the following expression,

$$c = c_0 / n. \tag{3.2}$$

Given that S(r, t) is the source function for diffusive light, for semi-infinite geometry as shown in Figure 3.1(a), the source function can be described by eq. 3.3 to express a positive and a negative optical sources:

$$S(r, t) = S_0 [\delta(r - z_0) - \delta(r + z_0)]. \tag{3.3}$$

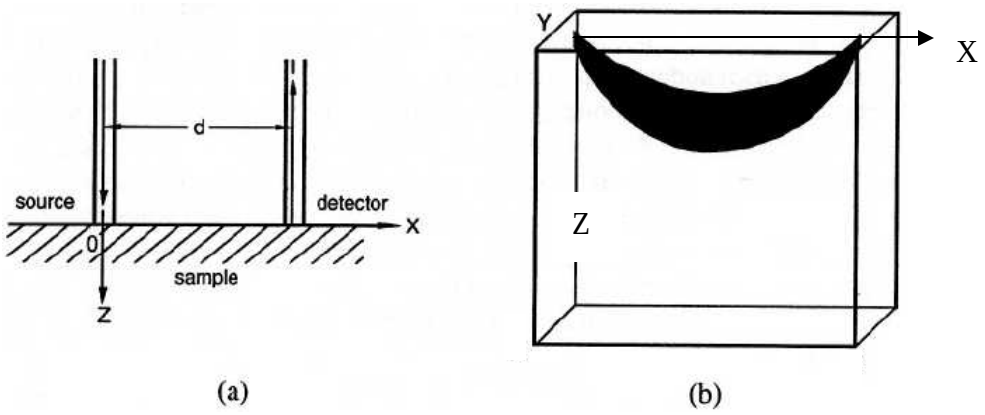

Figure 3.1 (a) Semi-infinite geometry for source and detector and (b) banana-shaped region of photon path distribution within the tissue [17]

Now, if the source light is of a continuous wave type, S_0 is a constant. For semi-infinite geometry, the desired photon-path-distribution function for photons injected at $r_0 = (0, 0, 0)$ and detected at $r_d = (d, 0, 0)$ is given by

$$P(x, y, z) = \frac{z^2 \exp(-k\{(x^2 + y^2 + z^2)^{1/2} + [(d - x)^2 + y^2 + z^2]^{1/2}\})}{(x^2 + y^2 + z^2)^{3/2}[(d - x)^2 + y^2 + z^2]^{3/2}} * [k(x^2 + y^2 + z^2)^{1/2} + 1]\{k[(d - x)^2 + y^2 + z^2]^{1/2} + 1\} \tag{3.4}$$

where k is defined as $k \cong 1/ L_a = (\mu_a/D)^{1/2} = (3\ \mu_a\ \mu_s')^{1/2}$. In a multiple-scattering regime, L_a determines the range of diffusive light migration. From the above equation, the peak position of the photon-path-distribution function P(x, y, z) within a cross section in the y-z plane for a fixed $0 < x < d$ can be determined. From symmetry it has $y = 0$, and if we take its z coordinate as $z_0(x)$, this function represents the modal line of the banana region [19], as plotted in Fig. 3.1(b).

In the weak absorption limit, which is a good approximation considering human tissue, where $kd << 1$, $z_0(x)$ is given by [16]

$$z_0(x) \cong [1/8(\{[x^2 + (d-x)^2]^2 + 32x^2(d-x)^2\}^{1/2} - x^2 - (d-x)^2)]^{1/2} \qquad (3.5)$$

At $x = d/2$ the modal line of the banana region reaches a maximum depth:

$$z_0^{max} \cong \frac{\sqrt{2d}}{4} \qquad (3.6)$$

3.1.1 Source Detector Separation vs. Depth of Penetration

As given by equation 3.5, the depth of penetration of light inside the biological tissue is dependent on the source-detector separation. This phenomenon is more clearly explained by Figure 3.2.

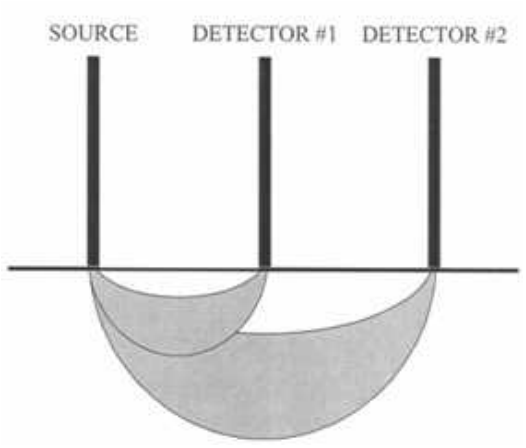

Figure 3.2 Different source-detector separations sample different depths of tissue. The shaded areas represent the average volume probed by the light for a given source-detector separation [20]

The average volume of tissue interrogated by the probe between the Source and Detector #1 is less than the volume interrogated by the probe between the Source and Detector #2. This phenomenon is of particular interest as the depth of penetration is directly related to the amount of information regarding the physiology happening within the biological tissue that can be obtained.

3.2 Experimental Method

A laboratory phantom experiment was done to validate the LCC – NIRS system and the new probe's functionality to detect Hb and HbO2 changes occurring inside the tissue. For this study, a static blood phantom was developed, and the measurements were taken while the blood was oxygenated and deoxygenated.

3.2.1 Static Blood Phantom Measurement

The experimental set up for this experiment included a cubical plastic container filled with a 3000-ml, 1% Intralipid solution and mixed with 85 ml of pure horse blood, which severed as the static tissue phantom. The probe was placed on one of the longer edges of the container, and the top of the container was covered using Para-film to prevent air from contacting the surface of the solution. The blood was initially deoxygenated by bubbling nitrogen gas into the solution. At first, the blood was fully deoxygenated by bubbling nitrogen gas for 4 hours, and then the measurement was started. After 1175 seconds (20 mins), bubbling of nitrogen was stopped, and the gas was switched to oxygen with a slow bubbling rate (to prevent the solution from forming too many bubbles).

3.3 Experimental Result

3.3.1 Results from the Static Blood Phantom Measurements

Figure 3.4 shows the filtered results obtained from the four detector channels. The filtering frequency was set at 0.05 Hz by empirical trials.

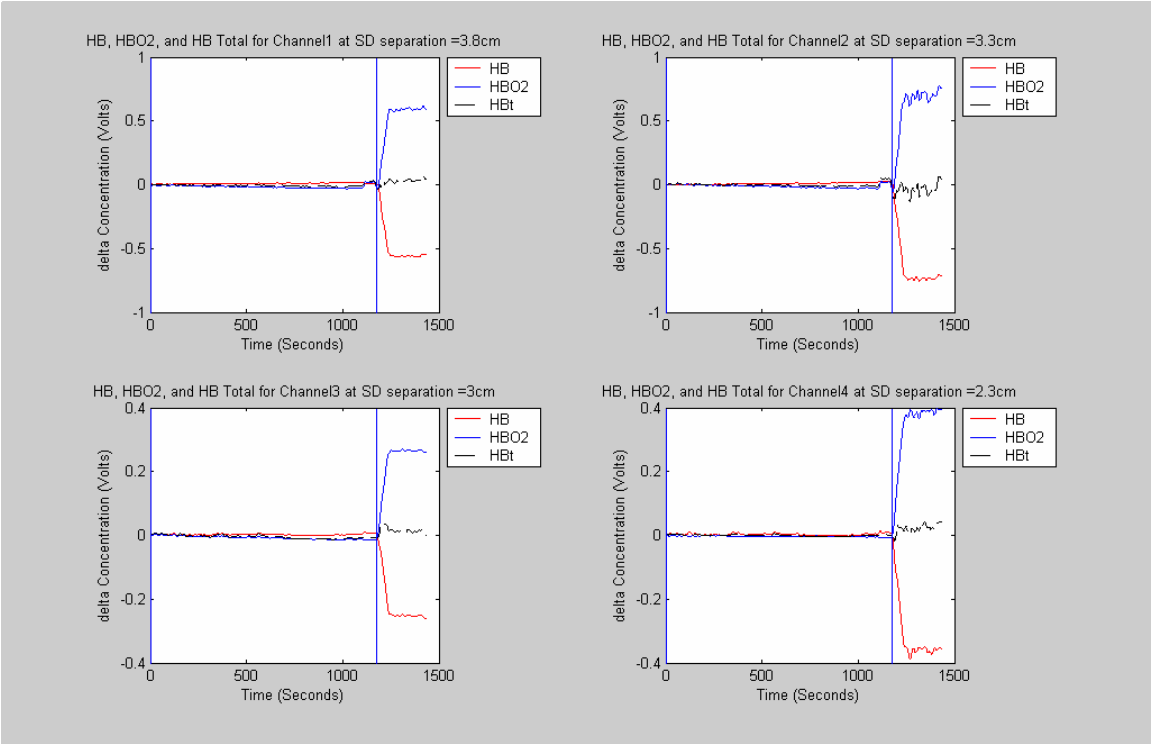

Figure 3.3 Plot of ΔHb, ΔHbO2 and ΔHbt for the static blood phantom

The baseline represents the case of deoxygenated blood in the solution, as the blood was fully deoxygenated by bubbling nitrogen gas for 6 hours before the measurement was started. The first blue marker in the above figure corresponds to the start of the measurement period. The second marker represents the time at which nitrogen gas was switched to oxygen gas. The slight deviation of the baseline just before the change of gas can be attributed to the process of switching the gas from nitrogen to oxygen. By close inspection on the plots, it can be seen that HbO2 concentration starts increasing and Hb concentration starts decreasing soon after the oxygen gas is switched on and the blood-Intralipid solution is oxygenated. The fact that the total hemoglobin concentration remains almost constant throughout the oxygenation process is clearly

evident for all channels, and this is what we expect to see if the NIR system operates and functions correctly.

CHAPTER 4

NEW APPLICATION 1: SCREENING TOOL FOR DETECTION OF SLEEP APNEA

4.1 Background of Sleep Apnea

Sleep-disordered breathing (SDB) is a condition of repetitive episodes of decreased or arrested respiratory airflow during sleep. Sleep disordered breathing consists of obstructive sleep apnea (recurrent interruptions of breathing during sleep), Hypopnea (shallow breaths during sleep), and upper airway resistance syndrome. Moreover, Obstructive Sleep Apnea/ Hypopnea Syndrome (OSAHS) is clearly defined by the occurrence of at least five, 10-second breathing pauses (apneas) or hypopneas (near apneas) per hour of sleep in association with sleepiness or at least two other major symptoms, including difficulty in concentrating, unrefreshing nocturnal sleep or nocturia. Snoring is also a strong marker for sleep apnea and upper airway resistance. Potentially modifiable risk factors for sleep-disordered breathing are overweight and obesity, alcohol, smoking, nasal congestion, and estrogen depletion in menopause [21].

An apnea involves upper-airway collapse and is defined as nearly complete cessation of airflow associated with oxygen desaturation or an arousal from sleep. Hypopneas are considered to exist on a pathologic continuum with apneas. Hypopneas are clinically more important because they may make up the majority of disordered breathing events in a given night, which are associated with partial collapse of the upper airway [22].

People with obstructive sleep apnea (OSA) have frequent and repetitive episodes of oxygen deficiency, experiencing momentary awakenings that result in sleep deprivation. The clinical symptoms include loud snoring and excessive daytime sleepiness. The intermittent abnormal deficiency of oxygen in the arterial blood (a condition known as hypoxemia) and episodes of brain activation (known as arousal states) are associated with abrupt increases in systemic blood pressure. The breathing pauses of sleep disordered breathing cause acute cardiovascular abnormalities. Apnea and episodes of hypopnea during sleep cause acute temporary changes in blood pressure, inducing elevations in mean arterial pressure (of 30 mmHg or more), fluctuations in heart rate and rhythm, increased sympathetic nerve activity, arousal and sleep fragmentation, and swings in pressure within the cavity of the chest. Sleep disordered breathing has been linked to considerable behavioral abnormalities, including excessive daytime sleepiness, decreased cognitive function, depression, as well as motor vehicle accidents and decreased quality of life. Excessive daytime sleepiness is a cardinal feature of clinically recognized sleep disordered breathing [21].

Men have a higher risk for obstructive sleep apnea than women do. The reason for this is not entirely clear, but hormonal influences may offer a partial explanation. Postmenopausal women are at higher risk for obstructive sleep apnea than premenopausal women, an effect that hormone replacement therapy may ameliorate [22].

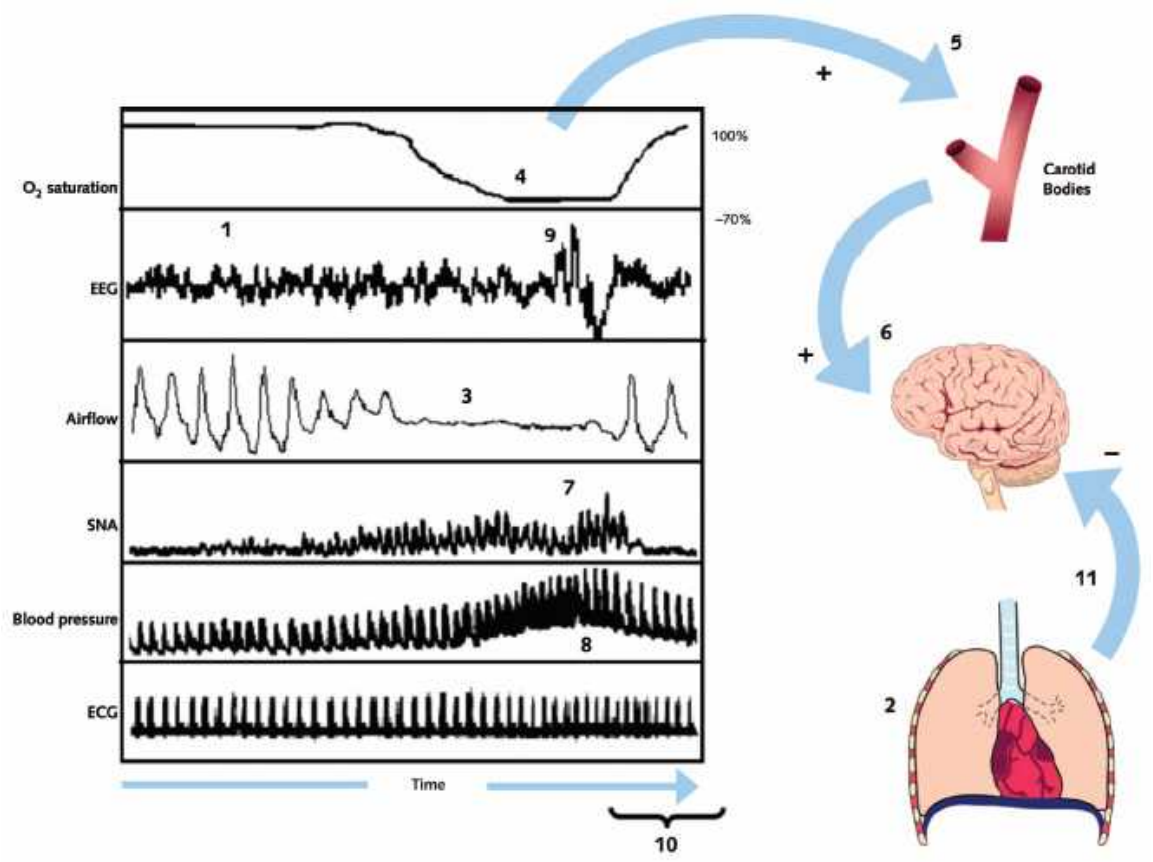

Figure 4.1. Polysomnagraphic data of an OSA patient [22]

Figure 4.1 shows the representative data of an OSA patient and the pathophysiology of OSA [22]. "In legend, numbers in parentheses correspond to the numbers shown in the figure. Sleep onset is heralded by electroencephalography (*EEG*) wave slowing (*1*) and a reduction in minute ventilation (*2*). In persons with obstructive sleep apnea, there is a reduction in their oxy-hemoglobin saturation (O_2 *saturation*) (*4*), due to the cessation of airflow resulting from the progressive collapse of the upper airway (*3*), and consequent stimulation of peripheral chemoreceptors, the carotid bodies (*5*). Chemoreflex stimulation acts through the central nervous system (*6*) to increase sympathetic neural activity (*SNA*), which is recorded peripherally as microneurographic

bursts (*7*). Blood pressure (*8*) increases as the apnea progresses. The exact mechanisms are not clear, but the apnea terminates with a central nervous system arousal, which is marked by an increase in electroencephalographic wave frequency (*9*). The far right portions of the tracings (*10*) show the cascade of events resulting from the arousal from sleep and restored upper-airway patency, including temporary supranormal ventilation, normalization of oxy-hemoglobin saturation, and instantaneous suppression of sympathetic nervous activity. During resumption of ventilation, sympathetic outflow is inhibited by afferents originating from thoracic mechanoreceptors, which synapse in the brainstem (*11*)" [22].

4.2 Protocol for Breath Holding Experiments

The experimental protocol was designed for Breath Holding as follows:

1. The human subjects taking the experiment were notified about the detailed procedures, and a consent form was signed by them.
2. The probe, designed for the LCC-NIRS system, was placed on the forehead of the human subject. The room was dark during the experiment to reduce interference due to ambient light.
3. The subject was instructed to keep the eyes closed for the entire experiment and to minimize any kind of motor activity like moving hands or talking.
4. The subject was instructed to relax for about 2 minutes, when the baseline was obtained.

5. The subject was asked to hold the breath, after exhalation, as long as possible before re-breathing.

6. The subject was asked to breathe normally for a period of about 2 minutes after the breath hold.

The protocol did not specify the time for the breath hold since everyone has a different capacity of holding breath. The subject was told to indicate when he/she started holding his/her breath and similarly indicate when he/she started re-breathing. The breath hold time ranged from 18 seconds to 39 seconds over multiple subjects. The study was done for 4 subjects, all male; all of them were volunteer students from UTA. An IRB approval was obtained from the office of research for this study. The approval form is attached in Appendix B.

4.3 Breath Holding Measurements Obtained from LCC-NIRS System

Four subjects were recruited for the breath holding study. The results of breath holding measurements were obtained from the LCC-NIRS device and shown as follows.

The first period of interest in the measurement is Baseline 1, i.e., the initial baseline before the 'Breath Hold' period. The second period is the 'Breath Hold' Period. The means and their respective Standard Deviation (SD) were calculated from the raw ΔHbt, $\Delta HbO2$, and ΔHb data for these two specific periods of measurement for each channel, respectively.

Figure 4.2 shows the filtered plots of ΔHb, $\Delta HbO2$ and ΔHbt, for Channel 2 with a source-detector separation of 3.3 cm, from the first subject. The 'Breath Hold' period is

19 seconds. The noisy signal was filtered using a fourth order Butterworth low pass filter, with a cut-off frequency of 0.06 Hz. The same filter was applied to all the other channels too. The first marker represents the time when the subject exhaled and started holding the breath. The second marker represents the time when the subject resumed breathing.

As seen in Figure 4.2, ΔHbO2 and Hbt start to increase as breath hold continues, and the increase continues even after the subject resumes breathing. Some time after normal breathing, the values of ΔHbO2 and ΔHbt come back gradually towards the baseline, but not completely reaching the baseline. ΔHb changes are not as noticeable as the other two parameter changes during the breath hold period. But ΔHb is rising throughout the measurement period.

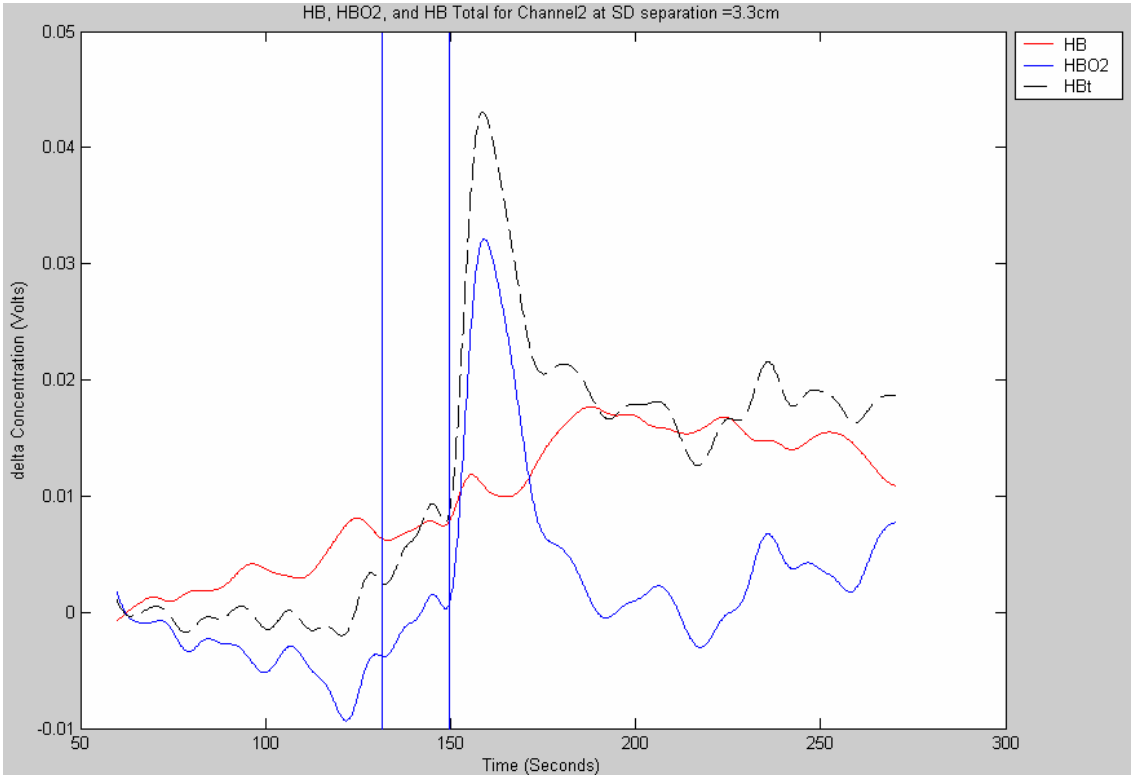

Figure 4.2 Subject 1 – Plot of ΔHb, ΔHbO2 and ΔHbt for Channel 2 for SD = 3.3 cm

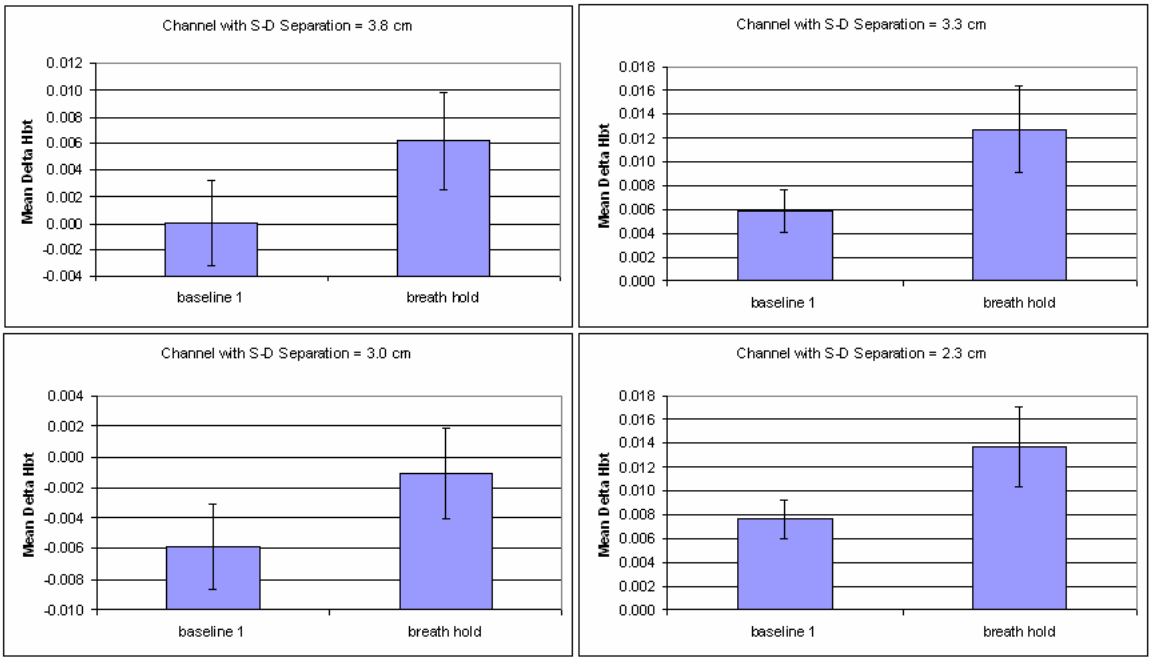

Figure 4.3 Subject 1 - Plot of Mean ΔHbt for all four channels

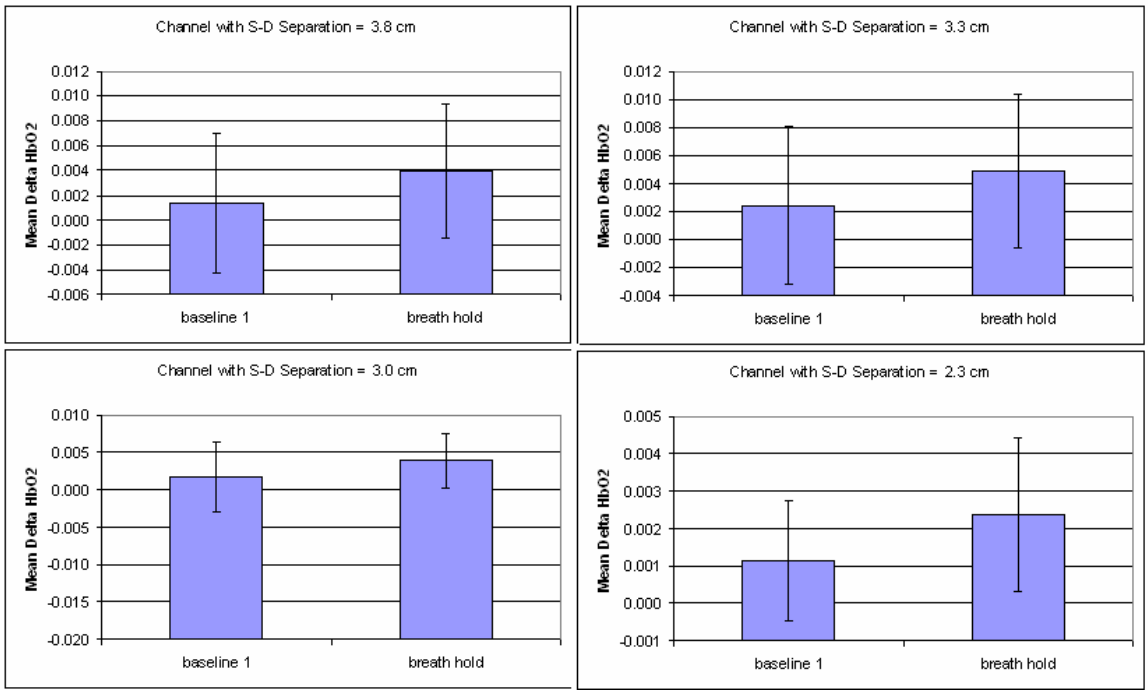

Figure 4.4 Subject 1 - Plot of Mean ΔHbO2 for all four channels

Moreover, it is seen from Fig. 4.2 that the period of about a minute after the subject resumes breathing, both ΔHbt and $\Delta HbO2$ are still increasing, and this observation is consistent for all channels. This phenomenon is possibly due to auto regulation of the human body to compensate for an increase in the pCO2 level in the brain during the 'Breath hold' period.

Mean values of ΔHbt and $\Delta HbO2$, along with their SDs, before and during 'Breath Hold' period were calculated and plotted for all four channels in Figs. 4.3 and 4.4, respectively. As seen from these two figures, all channels follow similar characteristics. The mean values of ΔHbt and $\Delta HbO2$ during 'Breath hold' are greater than the initial baseline values for all channels.

Figure 4.5 shows a filtered plot of ΔHb, $\Delta HbO2$ and ΔHbt for Channel 2 with a source-detector separation of 3.3 cm from the second subject. The 'Breath Hold' period is for 39 seconds. The noisy signal was filtered using a fourth order Butterworth low pass filter, with a cut-off frequency of 0.02 Hz.

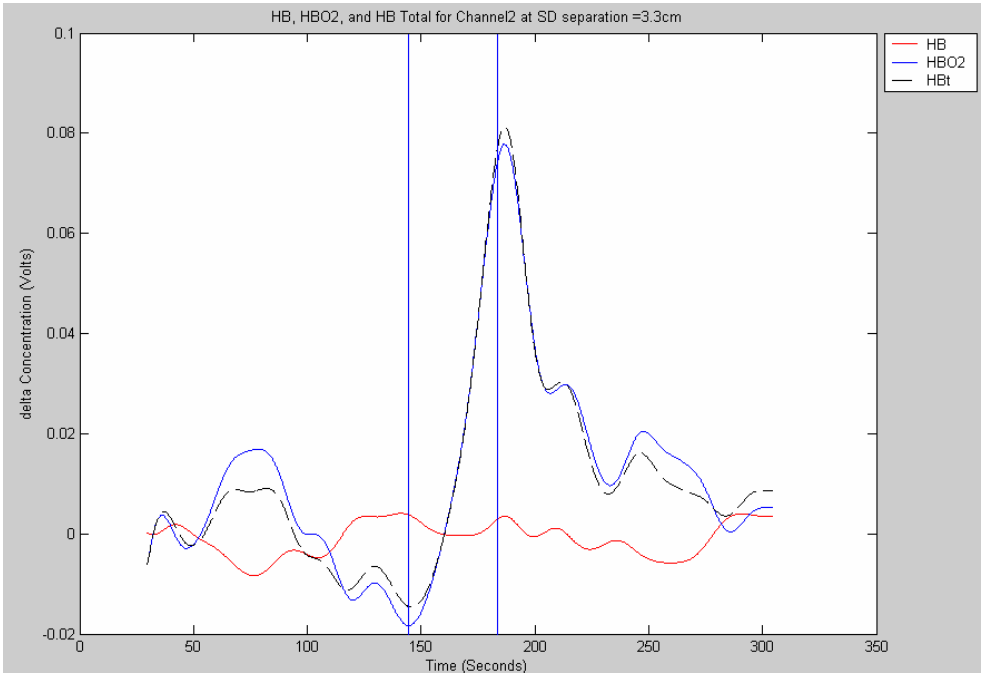

Figure 4.5 Subject 2 – Plot of ΔHb, ΔHbO2 and ΔHbt for Channel 2 for SD = 3.3 cm from subject 2

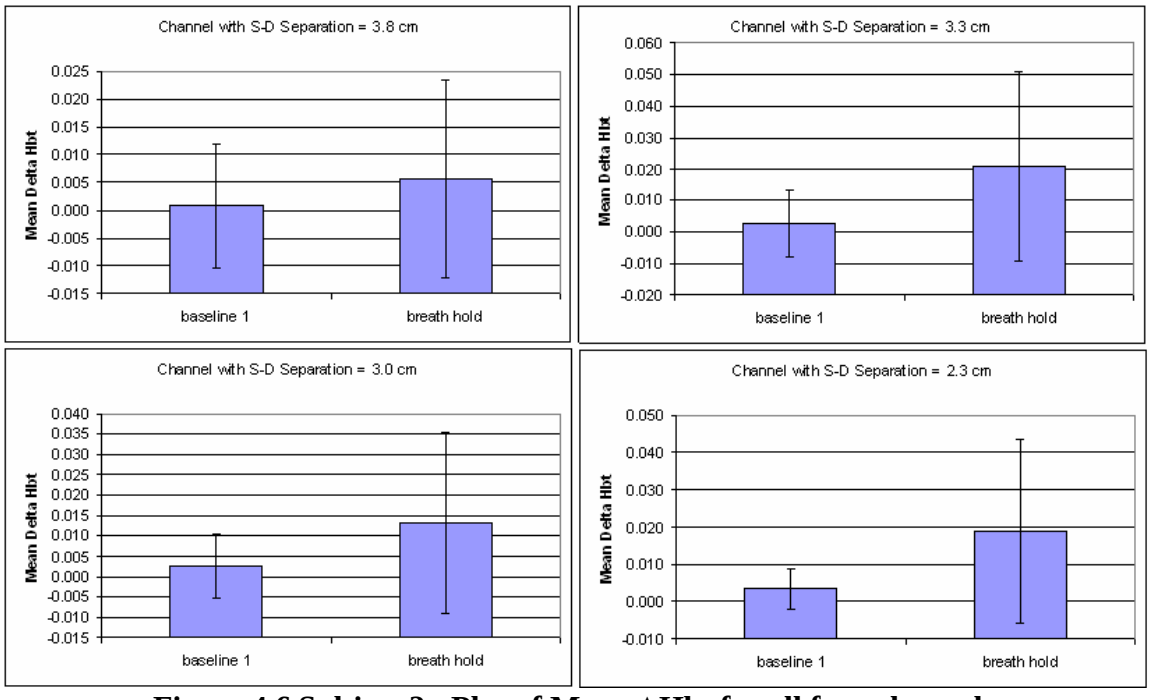

Figure 4.6 Subject 2 - Plot of Mean ΔHbt for all four channels

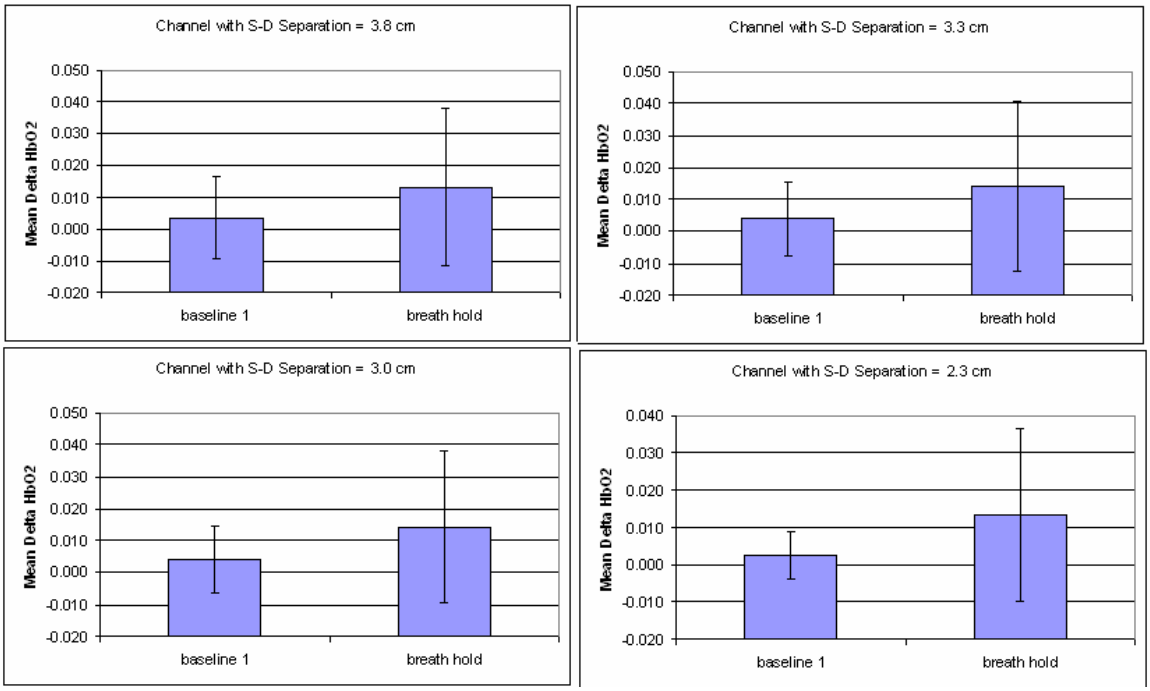

Figure 4.7 Subject 2 - Plot of Mean ΔHbO2 for all four channels

From Figures 4.6 – 4.7, it is clearly evident that for all channels, the ΔHbt and ΔHbO2 values from the second subject closely follow the first subject's traces in ΔHbt and ΔHbO2. Namely, both ΔHbt and ΔHbO2 start to increase as breath hold starts and continues, and the increase continues even after the subject resumes breathing. Some time after normal breathing, the values of ΔHbO2 and ΔHbt come back gradually towards the baseline.

Similarly, Figure 4.8 shows filtered plots of ΔHb, ΔHbO2 and ΔHbt, for Channel 2 with a source-detector separation of 3.3 cm, from the third subject. The 'Breath Hold' period was 30 seconds, and the noisy signal was filtered using a fourth order Butterworth low pass filter, with a cut-off frequency of 0.025 Hz.

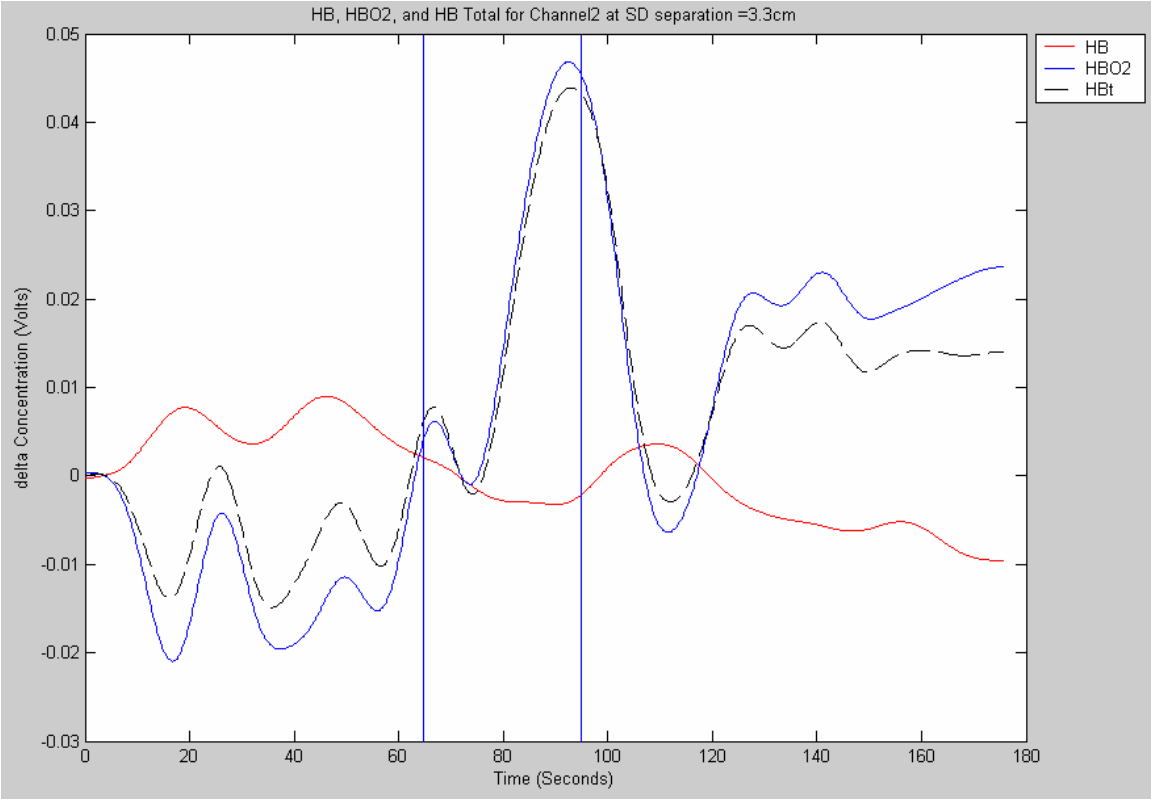

Figure 4.8 Subject 3 – Plot of ΔHb, ΔHbO2 and ΔHbt from Channel 2 for SD = 3.3 cm

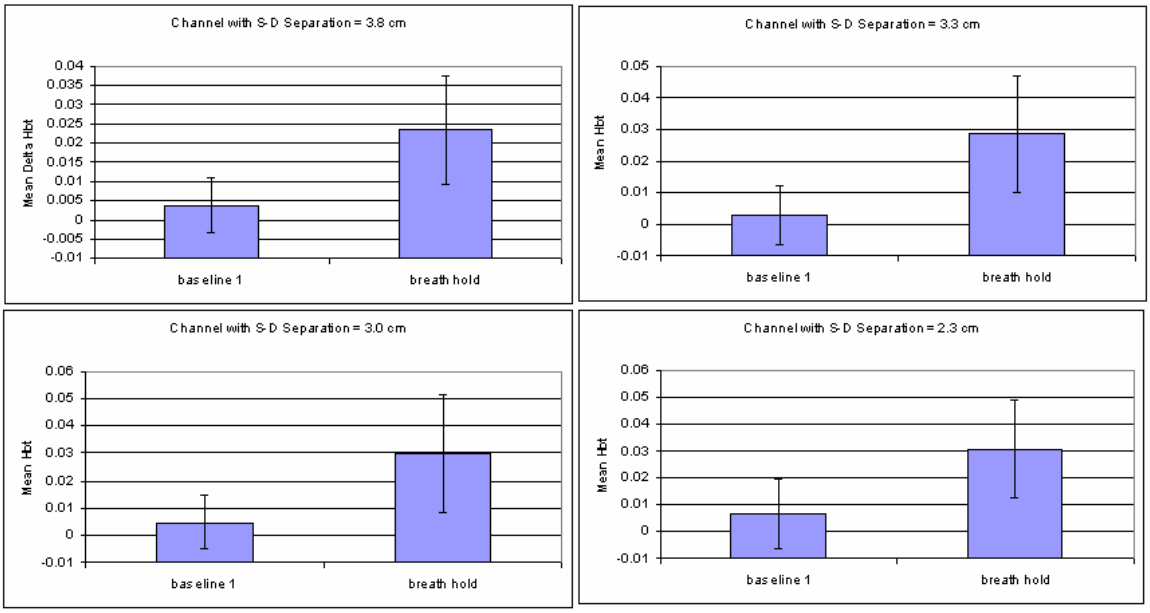

Figure 4.9 Subject 3 - Plot of Mean ΔHbt for all four channels

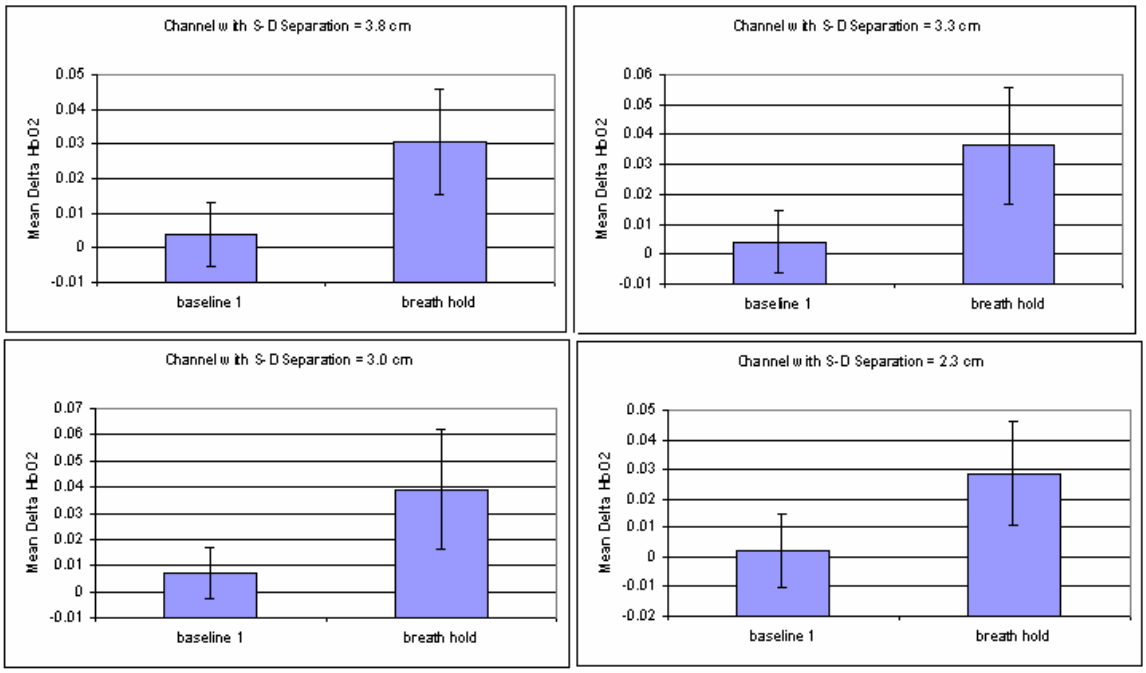

Figure 4.10 Subject 3 - Plot of Mean ΔHbO2 for all four channels

The mean ΔHbt and ΔHbO2 values from subject 3 before and during "breath hold" are summarized in Figs. 4.9 and 4.10 for all four channels, in accordance with the other two subjects' data. The ΔHbt and ΔHbO2 values for the third subject closely follow the first subject's changes in Hbt and HbO2.

Figure 4.11 shows the filtered plot of ΔHb, ΔHbO2 and ΔHbt, for Channel 2 with a source-detector separation of 3.3 cm from the fourth subject. The 'Breath Hold' period is for 26 seconds. The noisy signal was filtered using a fourth order Butterworth low pass filter, with a cut-off frequency of 0.02 Hz.

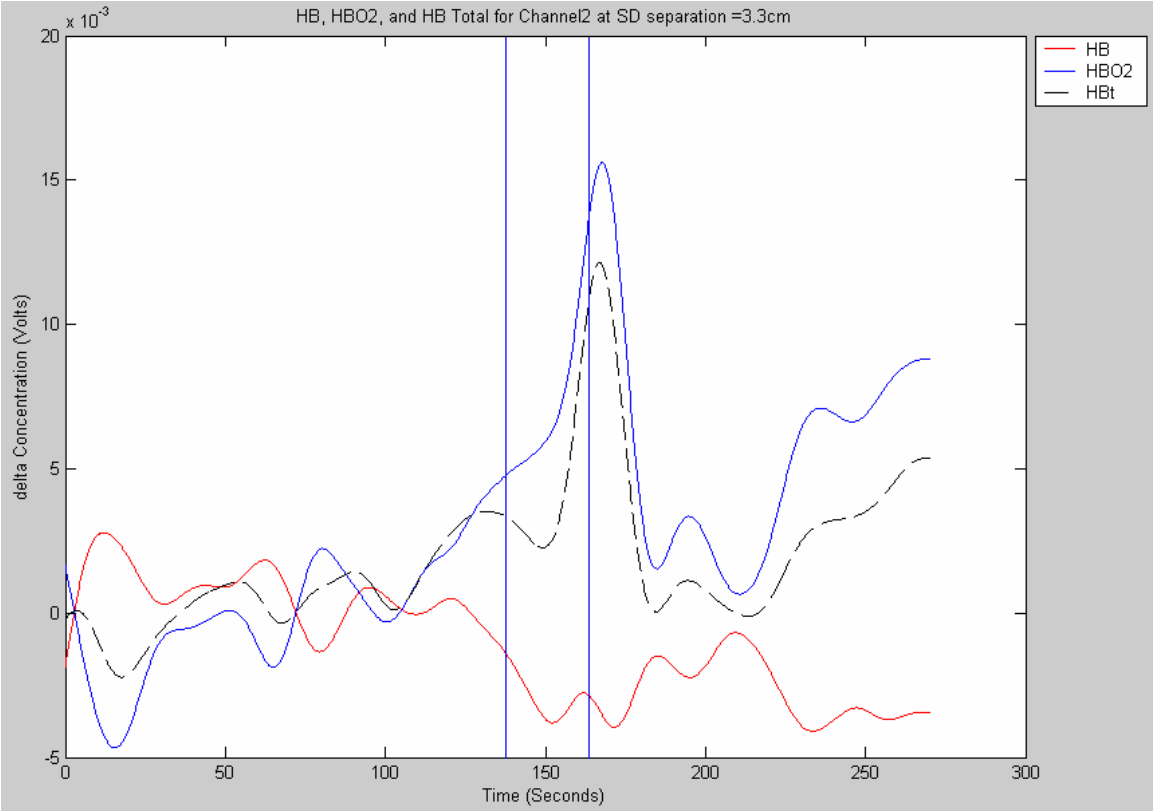

Figure 4.11 Subject 4 – Plot of ΔHb, ΔHbO2 and ΔHbt from Channel 2 for SD = 3.3 cm

Similarly, the mean ΔHbt and ΔHbO2 values for subject 4, from all four channels, are plotted in Figs. 4.12 and 4.13, respectively, along with their SD values. The trends shown in these two figures are consistent with those shown in other subjects' data (namely, Figs. 4.3-4.4, 4.6-4.7, and 4.9-4.10).

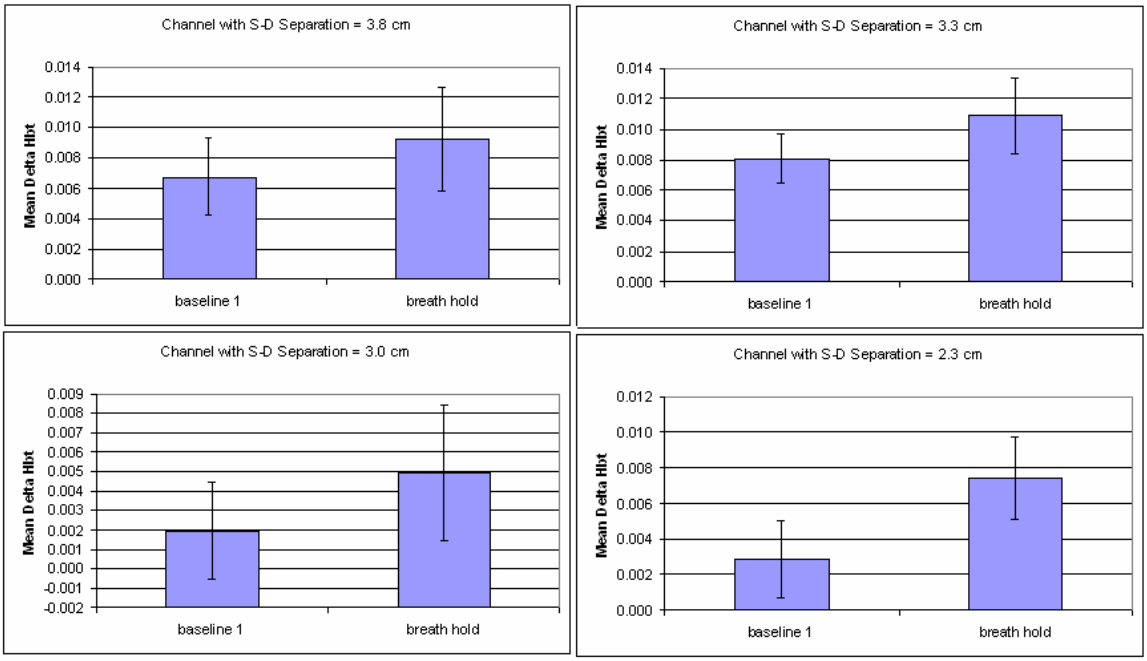

Figure 4.12 Subject 4 - Plot of Mean ΔHbt for all four channels

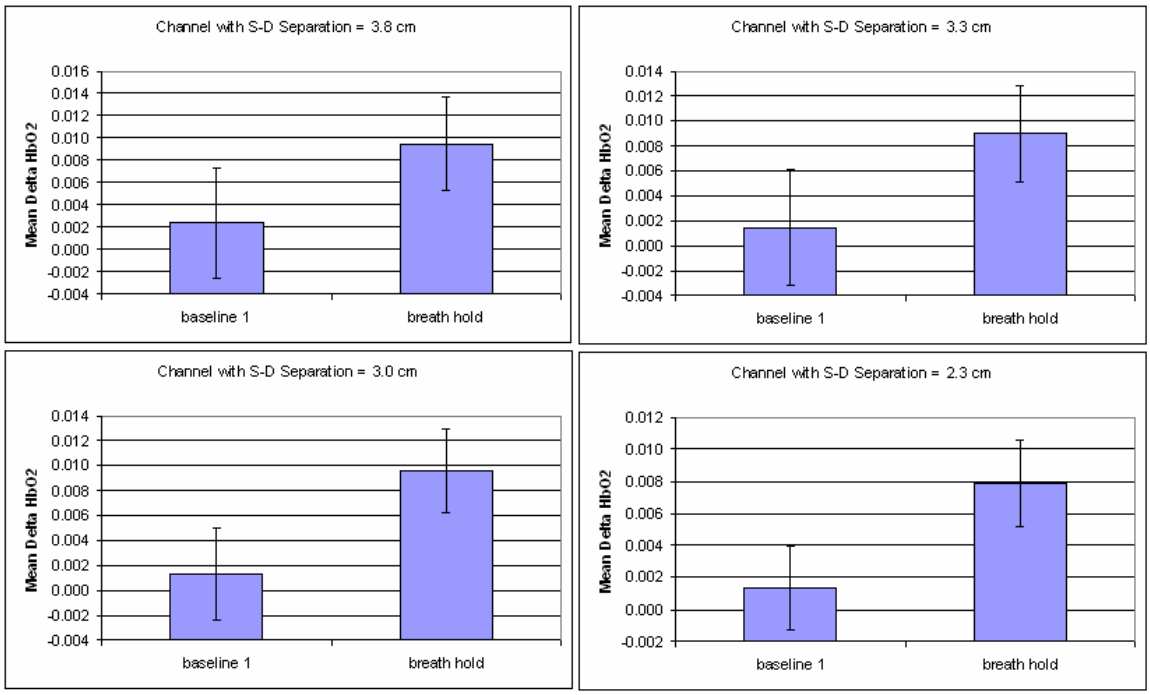

Figure 4.13 Subject 4 - Plot of Mean ΔHbO2 for all four channels

Furthermore, student T-test was done, for all subjects, to verify that there was a significant difference between the average baseline readings and the average breath hold readings of Hbt and HbO2 for all the channels, respectively. The results from the T-test, for all subjects, indicate that there is a significant difference between the baseline readings and the breath hold readings of Hbt and HbO2 for all the channels.

4.4 Data Obtained with LEDI Imager

In previous breath holding studies with cerebral hemodynamic changes, a commercial system (LEDI) was used. This system was manufactured by NIM (Near Infrared Monitor) Inc. (Philadelphia, PA). The LEDI Imager is a 16-channel imager comprising of four of dual-wavelength LED sources and ten detectors. The source-detector separation of 2.5 cm is fixed [15]. For comparison, the data was obtained using this imager for the same breath holding protocol as described above and shown as follows:

Figure 4.14 shows the plot of ΔHb, ΔHbO2 and ΔHbt (ΔBV) for Channel 5 through Channel 8. The subject under consideration is a different subject than the ones discussed in the previous section. The 'Breath Hold' period is for about 18 seconds. The first marker represents the time when the subject exhaled and started holding the breath. The second marker represents the time when the subject resumes breathing. As seen in this figure, ΔHbO2 and ΔHbt (ΔBV) start to increase as breath hold continues, and the increase continues even after the subject resumes breathing. Some time after normal breathing, the values of ΔHbO2 and ΔHbt (BV) come back gradually towards the

baseline. ΔHb changes are not as noticeable as the other two parameter changes during the breath hold period. All the other channels also follow the similar characteristics. Figure 4.15 show the plot of ΔHb, ΔHbO2 and ΔHbt (ΔBV) for Channel 9 through Channel 12. In order to measure the same area near the center of the forehead for better comparison between the two systems (i.e., LEDI and our LCC-NIRS system), the data from the other channels on the side of the LEDI were not included for analysis. The basic conclusion is that the measured values and trends of ΔHb, ΔHbO2 and ΔHbt using both the LEDI and our LCC-NIRS system are consistent with one another, supporting the functionality of our LCC-NIRS system and the new probe developed.

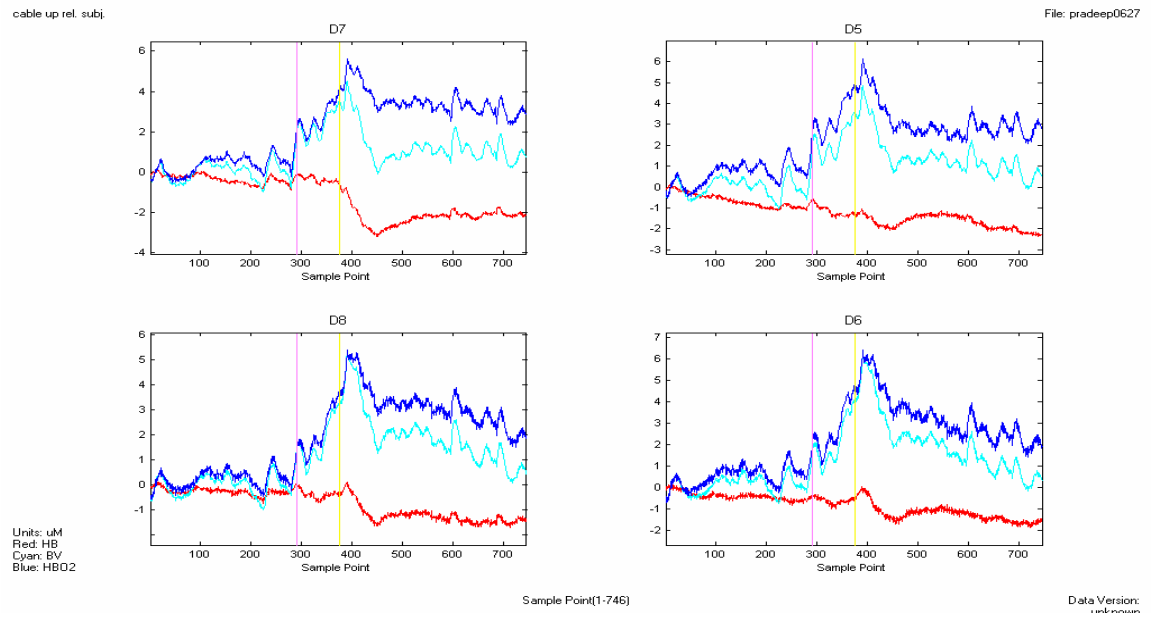

Figure 4.14 Plot of ΔHb, ΔHbO2 and ΔHbt for Channel 5 – Channel 8 [14]

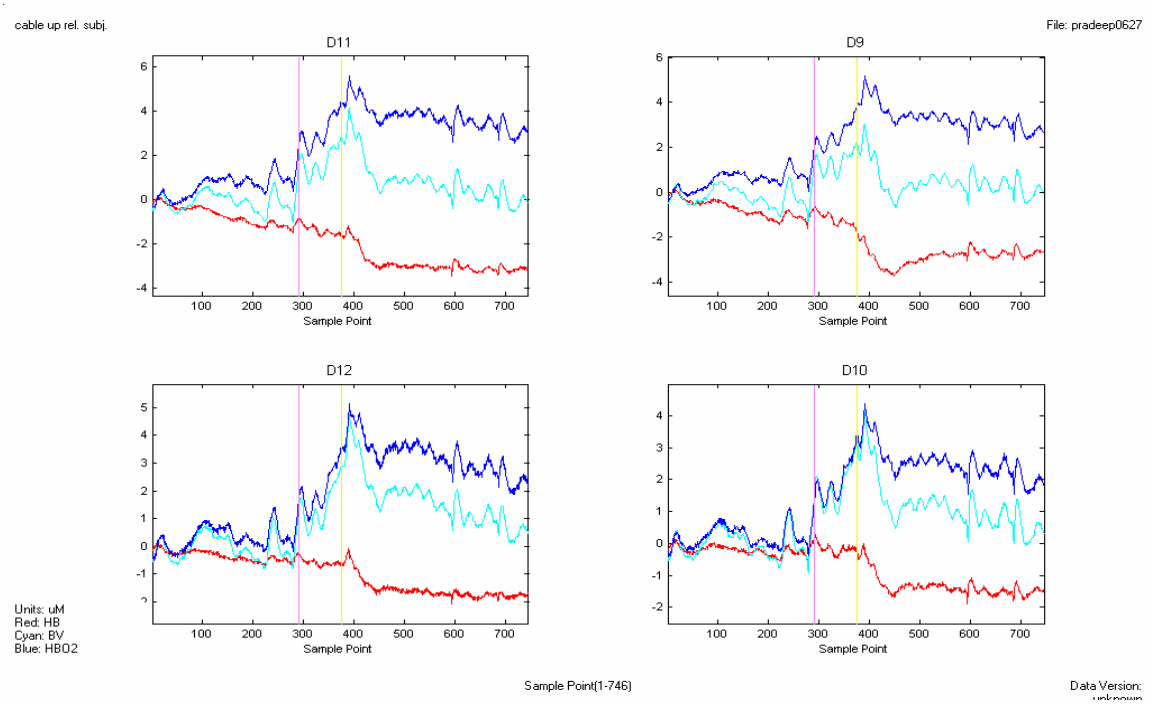

Figure 4.15 Plot of Hb, HbO2 and Hbt for Channel 9 – Channel 12 [14]

4.5 Analysis

During the breath hold period, there is an initial dip in ΔHbt and ΔHbO2 and then followed by an increase, which may be attributed to the auto regulation feature of the nervous system. During the breath hold period, there exists an increase in the pCO_2 levels in the brain as CO_2 is not being exhaled out of the body. The brain is the first organ that is affected by the pCO_2 accumulation, which leads to vasodilation and an increase in global cerebral blood flow, due to auto regulation of the human nervous system [22-24]. Therefore, both Hbt and HbO2 start to increase as breath hold continues, and the increase continues even after the subject resumes breathing, as the subject recovers from the lack of oxygen during the period of breath hold. Some time after normal re-breathing, the values of ΔHbO2 and ΔHbt come back gradually towards the post stimulus baseline,

which is generally different from the initial baseline. All these phenomena were correctly recorded by the LCC – NIRS for all of the subjects in my study.

Advantages of the LCC – NIRS System

The LCC - NIRS system is a multi separation, multi channel system, whereas the LEDI Imager is a fixed source-detector, multi channel system. Our LCC-NIRS device helps us probe different depths of the tissue, which possibly yields greater physiological meaning to the study being undertaken. Another good feature of the LCC – NIRS system is that the size of the probe that I developed can be placed at most places on the body. The data obtained by the LCC – NIRS system follows a similar pattern to the data that was obtained with the LEDI Imager as seen in the previous section. It was concluded from the results that the Near Infrared Spectroscopy System with the multi source-detector separation probe developed is capable of measuring hemodynamic changes occurring inside the human skull, on the pre-frontal lobe, during a breath holding period. This gives us confidence to apply the LCC-NIRS system for brain activity studies, such as monitoring brain functions during mental cognitive tasks, even during physical exercises.

One clinical application is the use of this system as a screening tool for detection of sleep apnea syndrome. Obstructive Sleep Apnea (OSA) is associated with frequent and repetitive episodes of oxygen deficiency, which results in sleep deprivation to the patients suffering from this syndrome. As the system developed is sensitive to the changes in both blood oxygen levels (HbO2) and total blood volume (Hbt), as shown from the results in

the previous sections of this chapter, LCC-NIRS can be a good tool for detection of sleep apnea.

CHAPTER 5

NEW APPLICATION 2: DETECTION OF HOT FLASHES IN MENOPAUSAL WOMEN

5.1 Background and Physiology of Hot Flashes

The most reported symptom of menopausal transition is hot flashes. The phenomena of hot flashes are the major reason for seeking medical advice for menopausal women. This phenomenon of hot flashes can be best described as a subjective and transient sensation of heat. It is felt most commonly in the upper chest and head [25]. Although there is an increase in body temperature momentarily, the body temperature actually falls due to sweating and vasodilation due to the autoregulation feature of the body to reduce temperature. Thus, though there is a sensation of heat during the occurrence of hot flashes, they are often followed by chills [26].

The work efficiency, behavior and quality of life of a person can be affected by the frequent disturbances in sleep resulting in discomfort throughout the day as a result of all the symptoms occurring during night. Although hot flashes are a frequently discussed problem, there is not much known about the pathophysiology of hot flashes [27]. They are random events, which differ from person to person, varying both in their magnitude and frequency of occurrence [26]. The average duration of a hot flash is 4 minutes [26]. The other factors like psychological stress, weather, claustrophobia, consuming alcohol, spicy foods are reported by some women to trigger hot flashes [28-30].

In women, hot flashes are the most severe and frequent during early postmenopausal years [25]. Hot flashes also are a common feature in women, who have undergone

ovariectomy, and some women during pregnancy and immediately postpartum [28]. Moreover, hot flashes are a common problem in men who suffer from prostate cancer or undergo Androgen Deprivation Therapy (ADT) [29].

Physiology of Hot Flashes

If the body temperature increases, then the body sweats causing cutaneous vasodilation to cool down the temperature of the body. When the body temperature goes below the set point, the body starts to shiver, and cutaneous vasoconstriction occurs to conserve the heat in the body. Thus the temperature of the body revolves around a set point. A sudden perturbation of the body's temperature set point in the hypothalamus results in the occurrence of a hot flash event or episode [30]. Due to the occurrence of a sudden transient change in the local area of the body, there is a sensation of intense heat, cutaneous vasodilation, and sweating (heat loss responses). The pathophysiology behind the occurrence of this phenomenon has not been explicitly explained as yet, although there is proof of the existence of a thermoregulatory response as explained above. Other physiological changes that occur during a hot flash episode are rise in skin conductance, increase in heart rate and peripheral blood flow [28].

Hot flashes are affected by the glucose levels within the body. A study conducted on post menopausal women also suggested that, higher blood glucose level would help in reduction of the hot flash events significantly. Hot flash episodes also have an effect on neuronal degeneration and subsequently cognition [31].

Hot flashes are events possibly resulting from numerous complex changes occurring within the body. Therefore, more research has to be undertaken for us to understand the exact mechanisms or physiology causing these events.

5.2 Measurement of Hot Flashes Using Skin Conductance

There are different parameters that can be measured for hot flashes, such as sternal skin conductance, respiratory exchange ratio, skin temperature, core body temperature, sweat rate [29]. The only objective method used currently by the hot flash research community is the sternal skin conductance monitoring device, the Biolog instrument, which measures sternal skin conductance using skin electrodes [32]. This, in certain ways, is referred to as the gold standard for the measurement of hot flashes. The advantages of this system are non-invasive, ambulatory and compact. Moreover, the objective recordings undertaken with this system, yields data that is correlating well with the subjective measurement and specific to hot flashes so that there are no false readings.

5.2.1 Theory of Skin Conductance

Skin conductance is considered to be a function of sweat gland activity and skin pore size, both of which are controlled by the sympathetic nervous system. Sweat glands are activated when the sympathetic nervous system is aroused in response to stress or anxiety. As sweat is produced, the skin's capacity to conduct current is enhanced and the measured conductance is increased [33].

Basically there are two techniques in the history of electro dermal measurement. In one, current is passed through the skin, and the resistance to passage is measured; in the other

no current is delivered from external sources, but the skin itself is the source of electrical activity [33]. The basic principle involved in measuring Skin Conductance Level (SCL) between two points (electrodes) on the subject's skin surface is by providing a constant voltage of 0.5 V DC between the two points. SCL is the reciprocal of the electrical resistance between the two electrodes. The measurement unit is generally µMhos, which is the inverse of Ohms, the unit of electrical resistance.

5.2.2 Instrument Used (Biolog 3991x/1)

The 3991x/1-SCL BioLog recorder (UFI, Morro Bay, CA.) is a compact, ambulatory skin conductance data recorder used for measuring hot flashes im my study. It senses skin conductance through an input assembly with two male snaps at its lead ends that are connected to the electrodes, to be described in the next section, and placed on the subject's skin surface. The system provides a constant voltage (0.5 V DC) between the two electrodes placed on the skin surface, and the recorder records the subject's Skin Conductance Level (SCL) data over a range of 0.1 to 38.9 µmho. Figure 5.1 shows the picture of the 3991x/1-SCL BioLog recorder next to the NIRS probe.

Figure 5.1 Biolog 3991x/1 system and the electrodes being used along with the LCC – NIRS probe

The 3991x/1-SCL BioLog system has two operational modes: 'Subject Connected' and 'PC Connected'. When being operated in the Subject Connected mode, it allows the Biolog Recorder itself to record the subject's SCL between the two electrodes placed on the subject's skin surface. In the PC Connected mode, it allows the Skin Conductance Level (SCL) data to be downloaded onto the computer. The SCL data was analyzed using the Downloading and Plotting Software (DPS) provided with the system [32].

5.2.3 Electrodes Used

The electrodes used for this study are the Ag/AgCl reusable electrodes with an electrolyte cream that is applied on the skin surface to get better conductance readings. The main problem faced by the hot flash research community is that the manufacturing of the electrolytic cream developed for hot flashes have been discontinued [35]. Therefore, it was necessary to look for an alternate option. A new conducting cream was compounded by Dr. Ratka that provides effective recordings of the electro dermal activity in my study. This

cream was prepared by mixing 100 g of Velvachol cream (hydrophilic base), commercially available from Healthpoint (San Antonio) with 100 g of polyethylene glycol (PEG 400 – 600) and 0.76 g of Potassium Chloride [35].

5.3 Simultaneous Measurement for Hot Flash Detection

As discussed in section 5.1, blood rushes through the upper part of the body during a hot flash. Since the rush of blood is cutaneous, a large change in blood flow on the upper chest surface can be expected. Thus, measuring changes in blood flow and volume on the skin over the chest could provide useful information about hot flashes. As the LCC – NIRS system was shown to be sensitive to changes in blood flow and volume in Chapter 4, the same system and probe was used to detect the hot flashes. Moreover, as the probe that I developed has a greater penetrating depth than the skin depth, I expected the system to be able to detect hot flashes. I conducted a pilot study at the Institute for Aging and Alzheimer's Disease Research at the University of North Texas Health Science Center, Fort Worth. For this study, several subjects were recruited for the measurements, and all of them were menopausal women with current hot flashes. Four subjects had one or more hot flash episodes during the measurement, which lasted 1-1.5 hours.

5.3.1 Protocol Used

The LCC – NIRS probe and the skin conductance electrodes were placed on the subject's sternal skin area, as shown in Figure 5.2, for simultaneous measurements of the two devices. The measurement period was 1 to 2 hours. The subject reported the period of hot flashes by pressing the marker buttons on the SCL meter/recorder (Biolog 3991x/1). When

the subject pressed the buttons, I also noted manually the starting and ending time of the hot flash period as a reference for later comparison.

Figure 5.2 Placement of the LCC – NIRS probe and the skin conductance electrodes

5.3.2 Results and Analysis

The data obtained were analyzed using a MATLAB program (Appendix A). A fourth order low pass Butterworth filter (available in the MATLAB) was used to remove high frequency noise which could be due to heart rate or transient motion. The cut off frequency was chosen with trial and error method and was selected to be 0.03 Hz.

Figure 5.3 shows the NIRS data for all the hot flash events experienced by the first subject as recorded from one of the four channels (channel 3). Shown in the figure, the blue markers represent the start and end of the hot flash periods. The skin conductance data is shown on Figure 5.4 for the same subject, who experienced four hot flash events. The duration of each hot flash event is given in Table 5.1.

Table 5.1 Duration of hot flash events reported by subject 1

Number of Hot Flash Event	Duration of Event (Seconds)	
	SCR Recorder	NIRS
First	262	260
Second	187	210
Third	137	135
Fourth	247	248

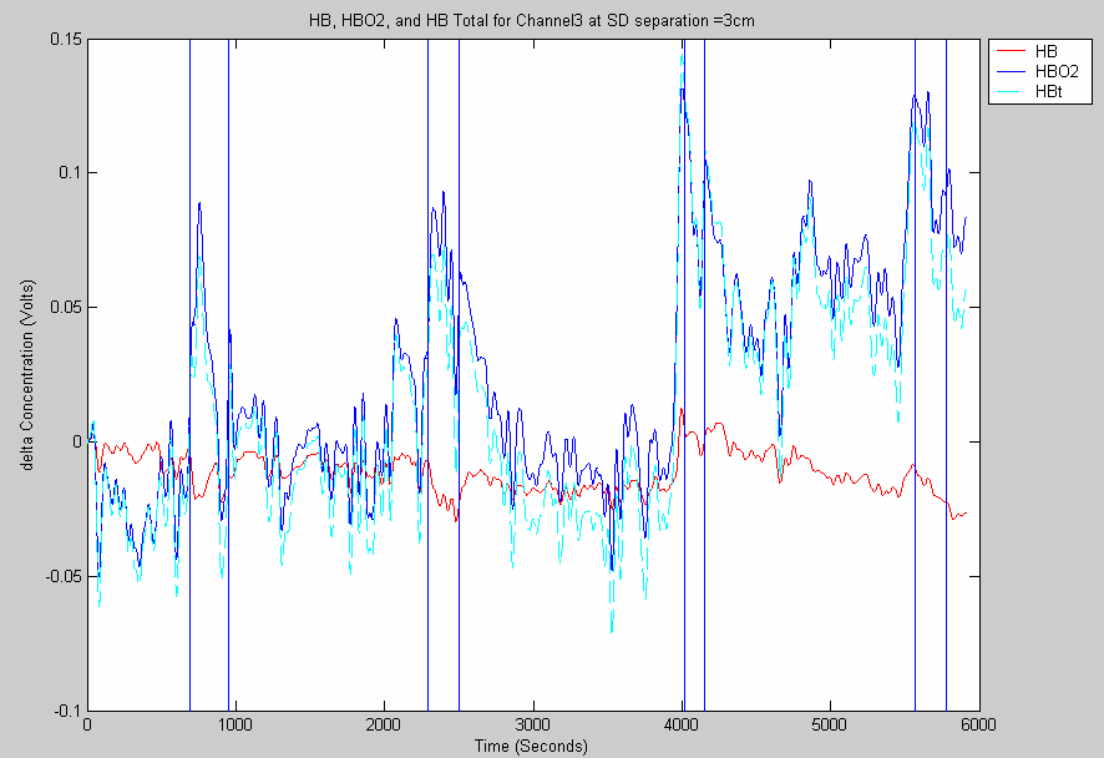

Figure 5.3 Subject 1 - Plot of ΔHb, ΔHb02, ΔHbt of 1 channel for all hot flash events

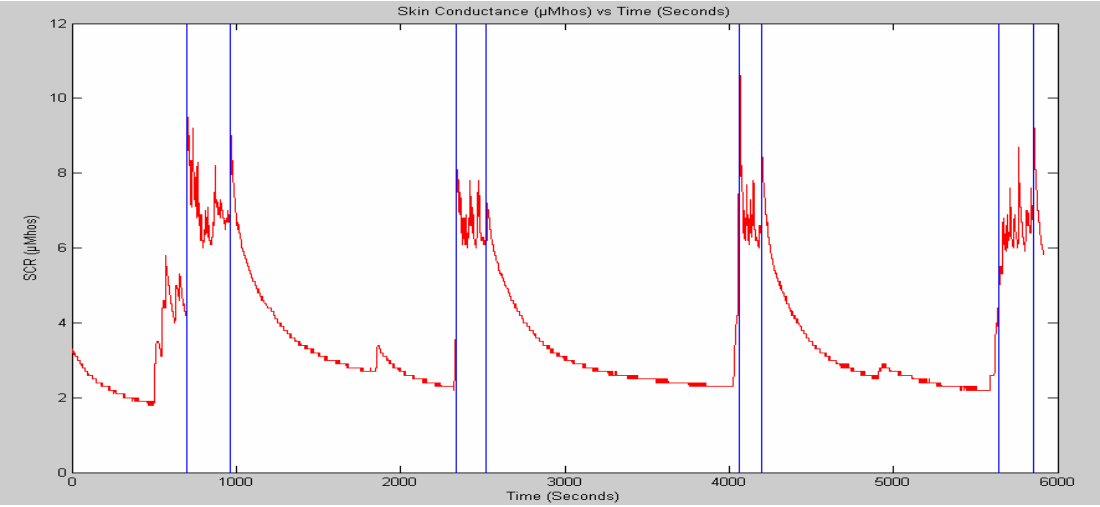

Figure 5.4 Subject 1– Plot of Skin conductance (µMho) vs. Time (Seconds)

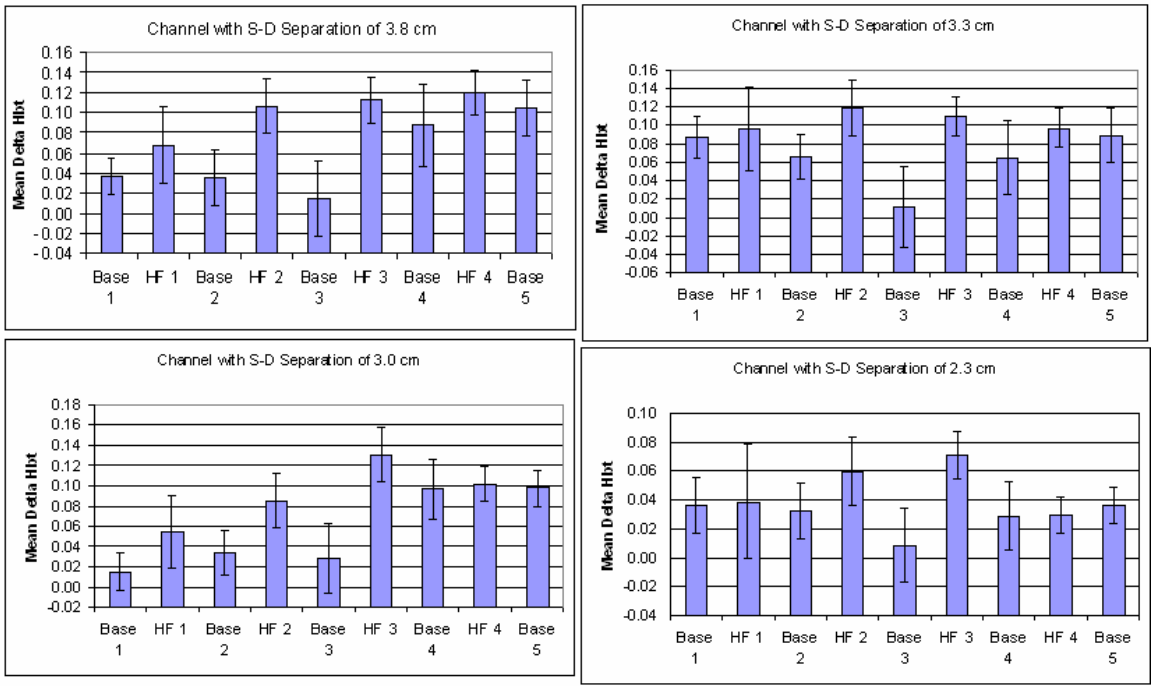

Figure 5.5 Plot of Mean ΔHbt for four detectors from Subject 1

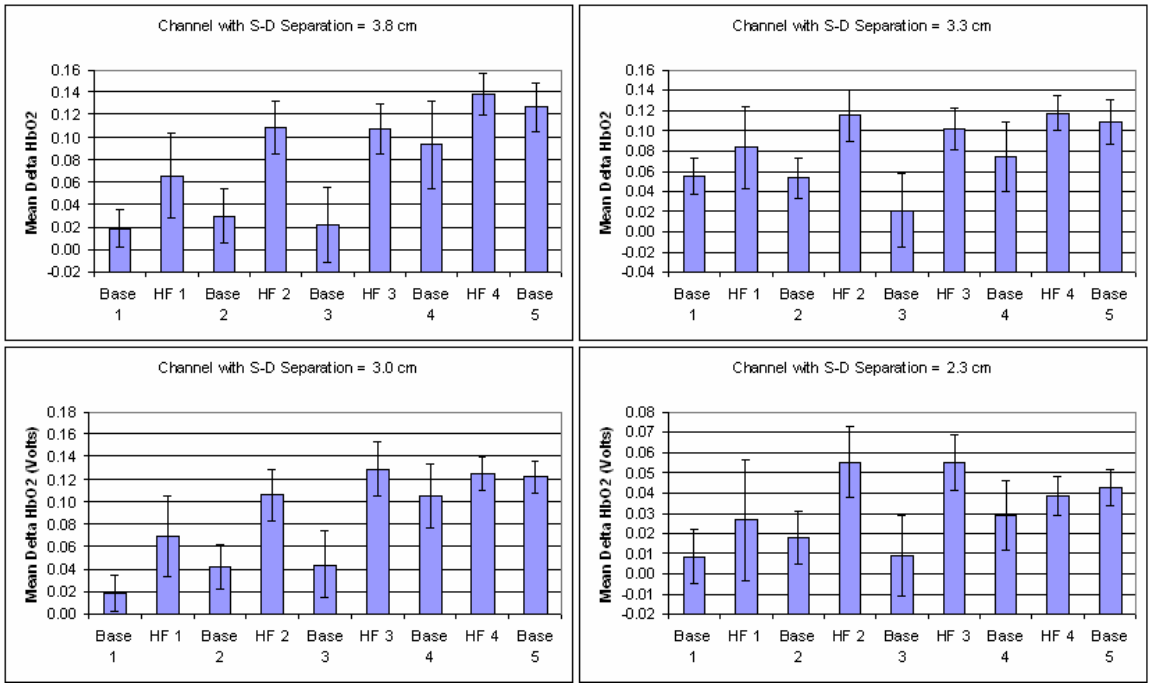

Figure 5.6 Plot of Mean ΔHbO2 for four detectors from Subject 1

Figures 5.5 and 5.6 shows the plot of mean ΔHbt and ΔHbO2, for the four detectors, for Subject 1. The error bars shown are the standard deviation for each region. All the detectors follow similar characteristics as seen from Figure 5.5 & 5.6. During the period when the subject experiences a hot flash event, as reported by the subject, there is an increase in the local blood flow (both ΔHbt and ΔHbO2) followed by a gradual decay toward the baseline after the hot flash is gone. This phenomenon is also in accordance with the changes in skin conductance as seen in Figure 5.4. ΔHb behaves in an opposite fashion from the other two parameters (ΔHbt and ΔHbO2) for all the detectors. The amplitude of ΔHb changes is relatively lower as compared to the changes in ΔHbt and ΔHbO2.

There was an increase in the baseline just after the third hot flash period. This can be attributed to a motion artifact, as the subject was talking and moving around in her chair continuously for the last 15 minutes of the measurement period. This was evident from the

data acquired from the LCC - NIRS system. The data obtained from both the systems matched for the time periods of the hot flashes as seen from Figures 5.3 and 5.4. Thus, the LCC – NIRS system is proven to be able to detect hot flash events accurately, while the noise shown in the NIRS data is high and needs to be minimized and improved in our future development.

The student T-test was done to verify if there was a significant difference between the average baseline readings and the average hot flash event readings of ΔHbt and ΔHbO2 for all the channels respectively. The T-test results indicate that there is a significant difference between the baseline reading and the hot flash readings of ΔHbt and ΔHbO_2 from all the respective channels.

Figure 5.7 shows the NIRS data for all the hot flash events experienced by the second subject as recorded by one of the channels (channel 3). The skin conductance data is as shown in Figure 5.8 for the same subject, who experienced two hot flash events. The duration of each hot flash event is given in Table 5.2.

Table 5.2 Duration of hot flash events reported by subject 2

Number of Hot Flash Event	Duration of Event (Seconds)	
	SCR Recorder	NIRS
First	323	331
Second	220	216

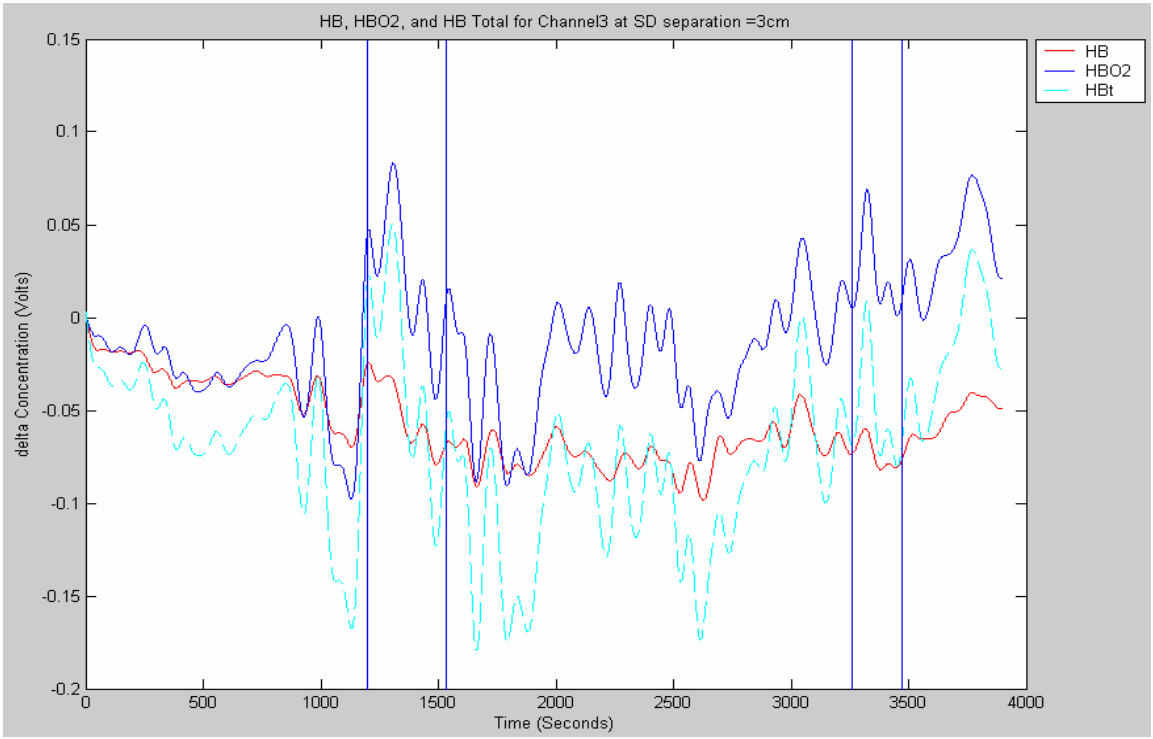

Figure 5.7 Subject 2 - Plot of ΔHb, ΔHb02, ΔHbt of 1 channel for all hot flash events

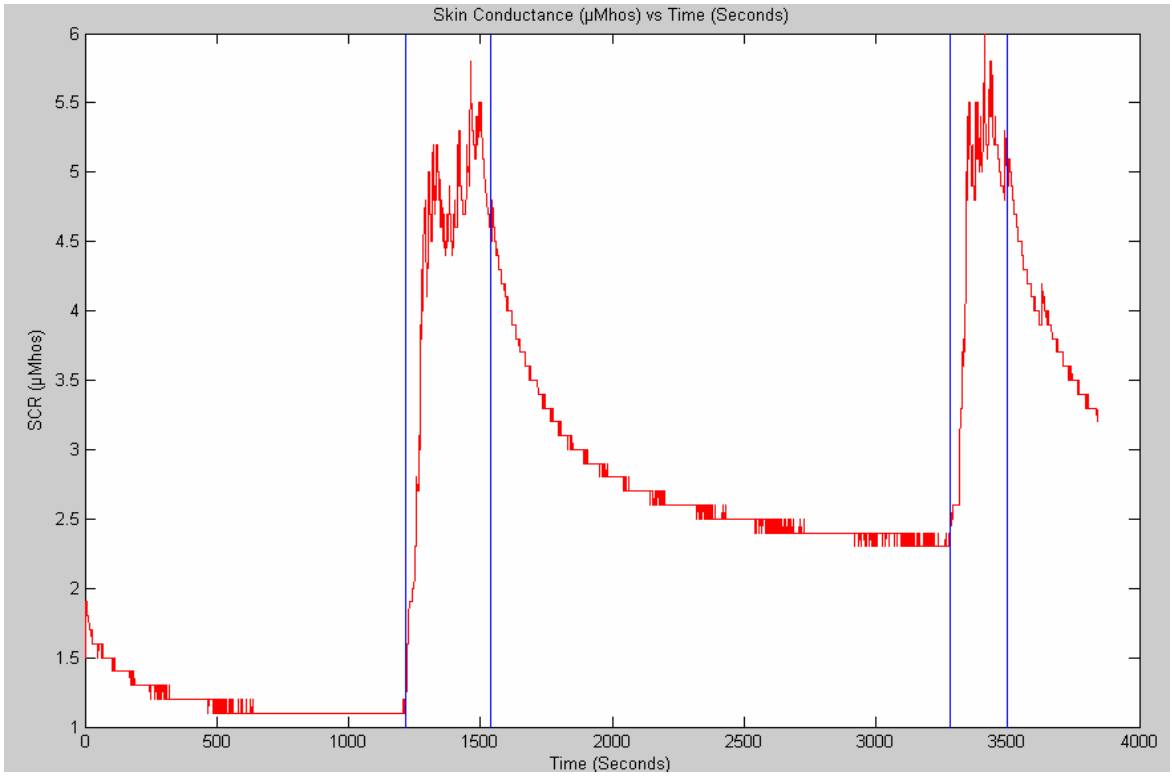

Figure 5.8 Subject 2– Plot of Skin conductance (µMho) vs. Time (Seconds)

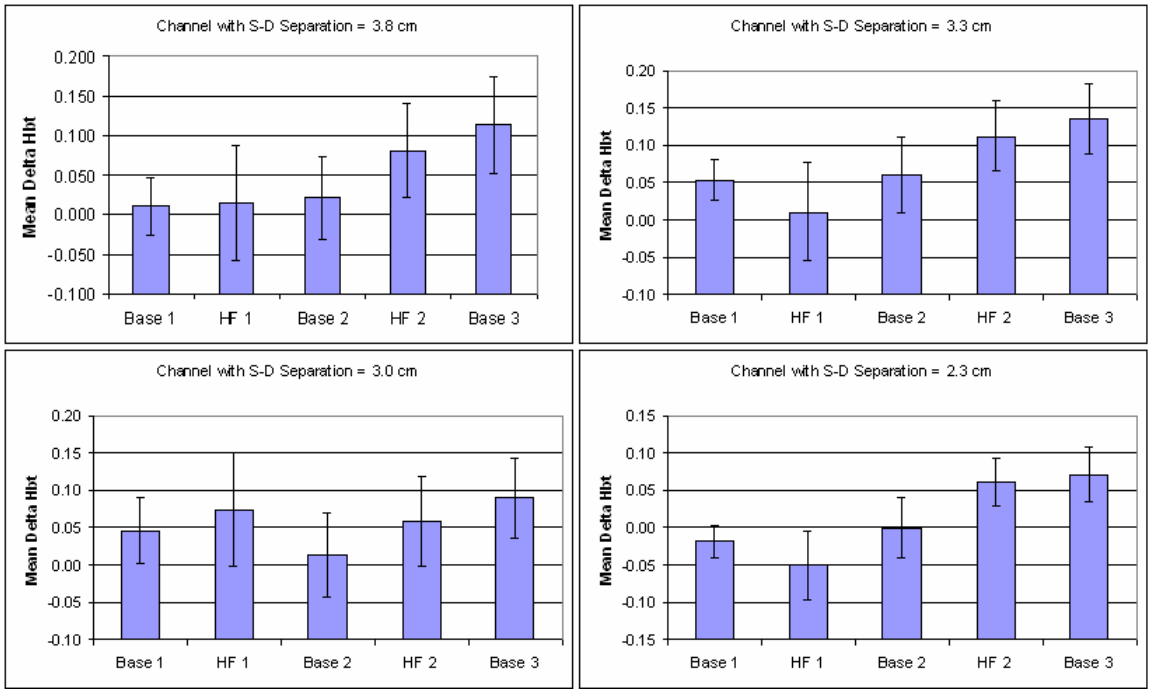

Figure 5.9 Plot of Mean ΔHbt for four detectors for Subject 2

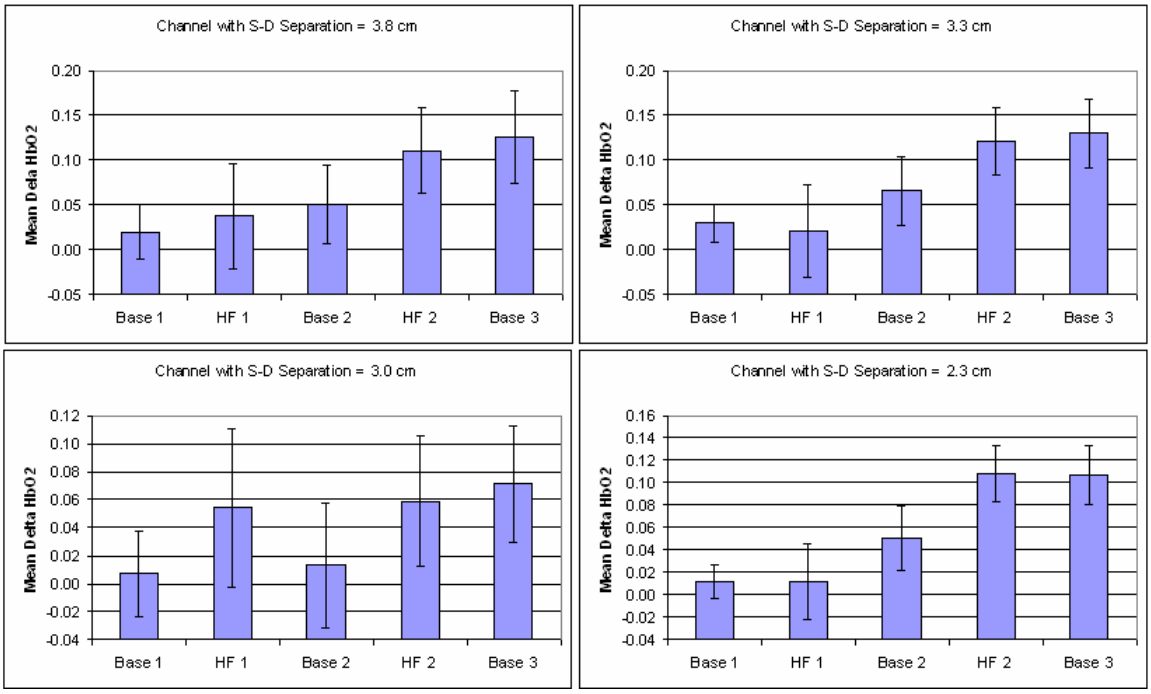

Figure 5.10 Plot of Mean ΔHbO2 for four detectors for Subject 2

Figures 5.9 and 5.10 shows the plot of mean ΔHbt and ΔHbO2, for four detectors, for Subject 1. The error bars shown are the standard deviation for each region. During this measurement, the channel with a source-detector separation of 3.0 cm detected the first hot flash event, while the other detectors seemed not to detect the first event by visual inspection. The second event was not shown very obviously in the NIRS data as can be seen from the Figures 5.9 & 5.10. This phenomenon can be attributed to the background noise present in the recording. This indicates that the system has to be further improved to eliminate the background noise.

It is noticed that the decay time of the skin conductance is slower than the NIRS parameters in returning to the baseline. This phenomenon is expected as skin conductance is considered a slow changing phenomenon. The LCC – NIRS is a system which is very sensitive to blood volume changes locally. Blood volume change in a local area is a faster response of the body. Therefore, the change in NIRS signals is faster than the skin conductance changes.

Furthermore, student T-test was done to verify that there was a significant difference of ΔHbt and ΔHbO2 for all the channels, respectively. The results from the student T-test indicate that there is a significant difference between the baseline reading and the hot flash readings for all the channels.

Figure 5.11 shows the NIRS data for all the hot flash events experienced by the third subject as recorded by one of the channels. The skin conductance data is shown on Figure 5.12 for the same subject, who experienced one hot flash event during the measurement. The duration of the hot flash event is given in Table 5.3.

Table 5.3 Duration of hot flash events reported by subject 3

Number of Hot Flash Event	Duration of Event (Seconds)	
	SCR Recorder	NIRS
First	242	240

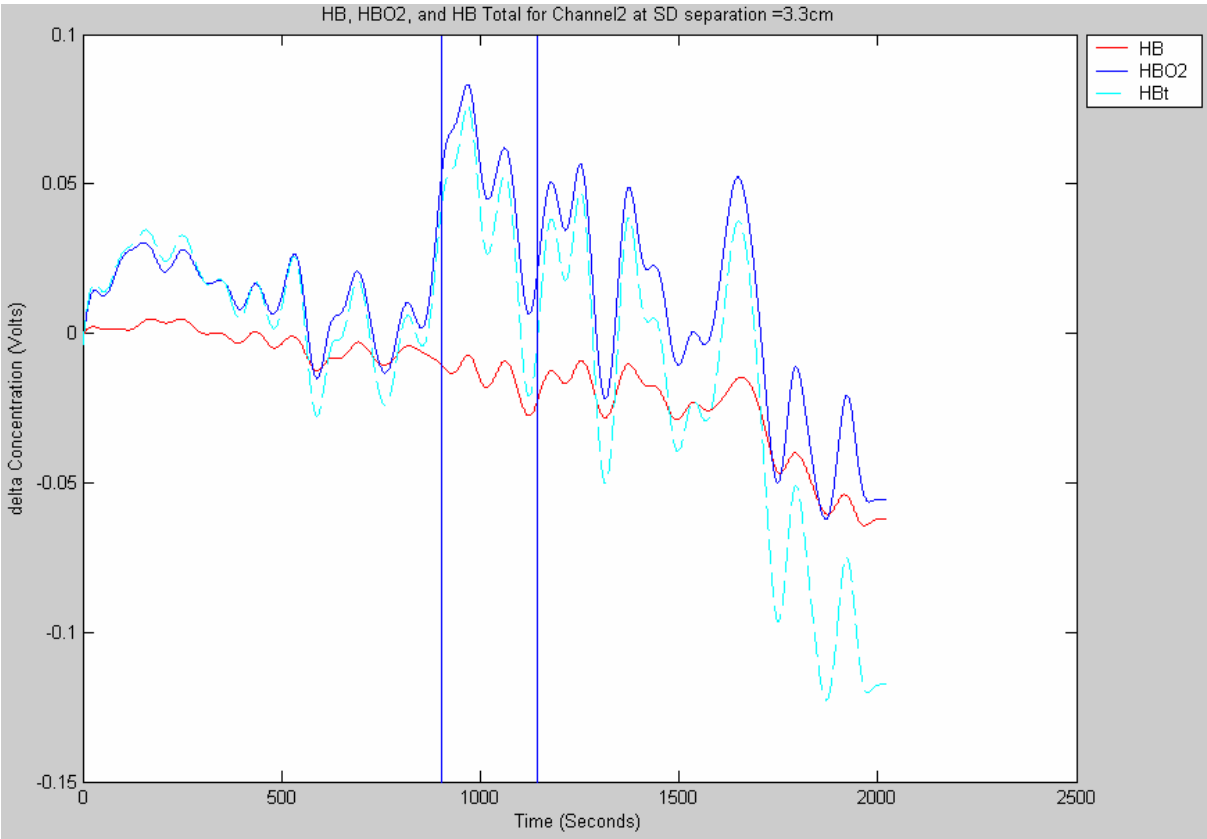

Figure 5.11 Subject 3 - Plot of ΔHb, ΔHb02, ΔHbt of 1 channel for all hot flash events

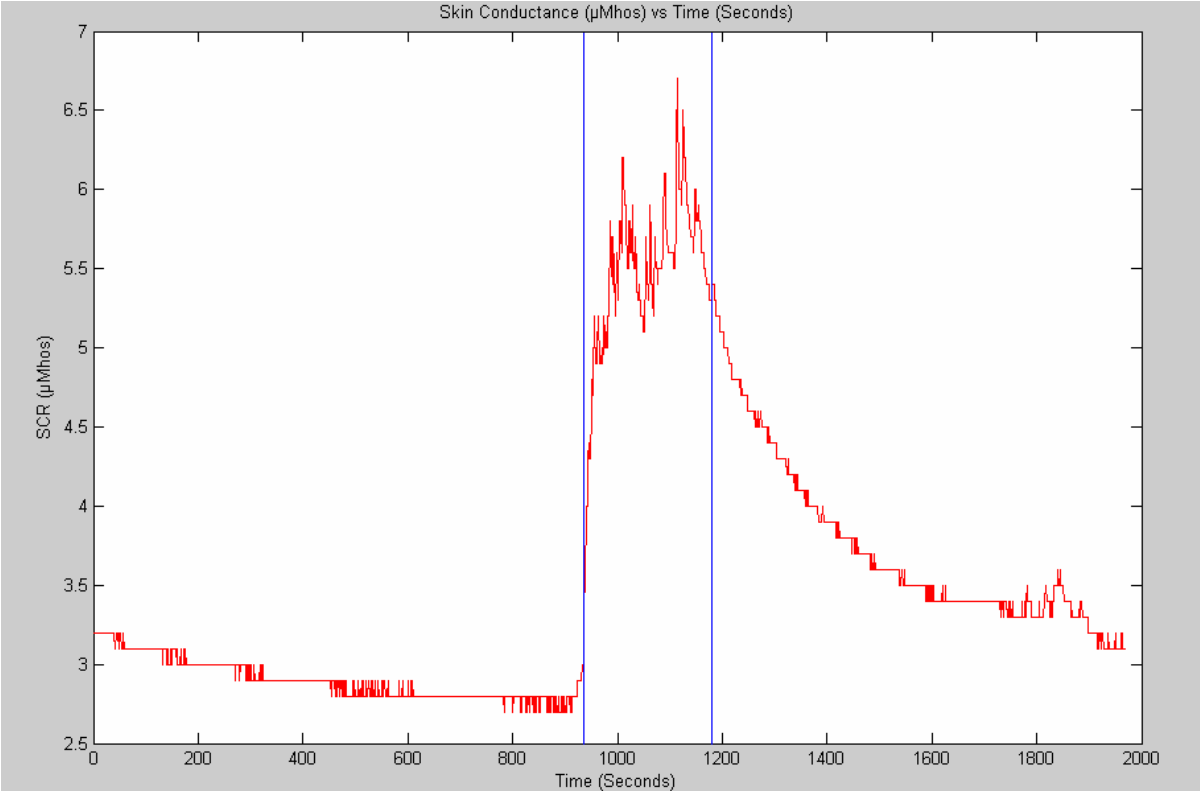

Figure 5.12 Subject 3– Plot of Skin conductance (µMho) vs. Time (Seconds)

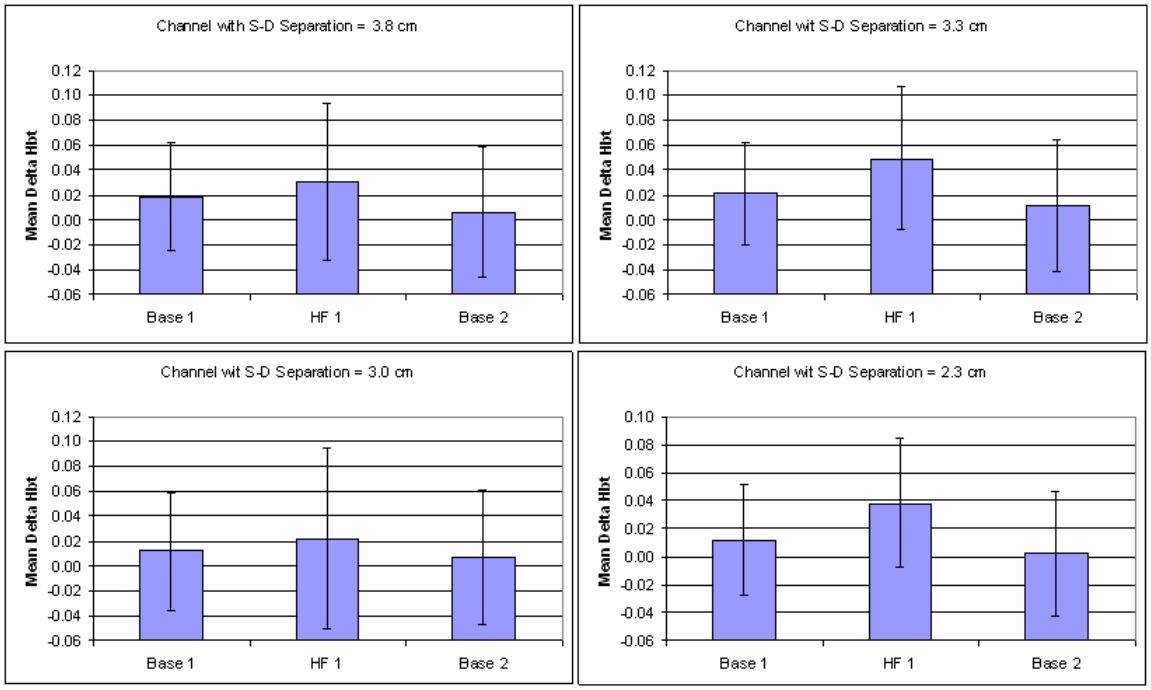

Figure 5.13 Plot of Mean ΔHbt for all detectors for Subject 3

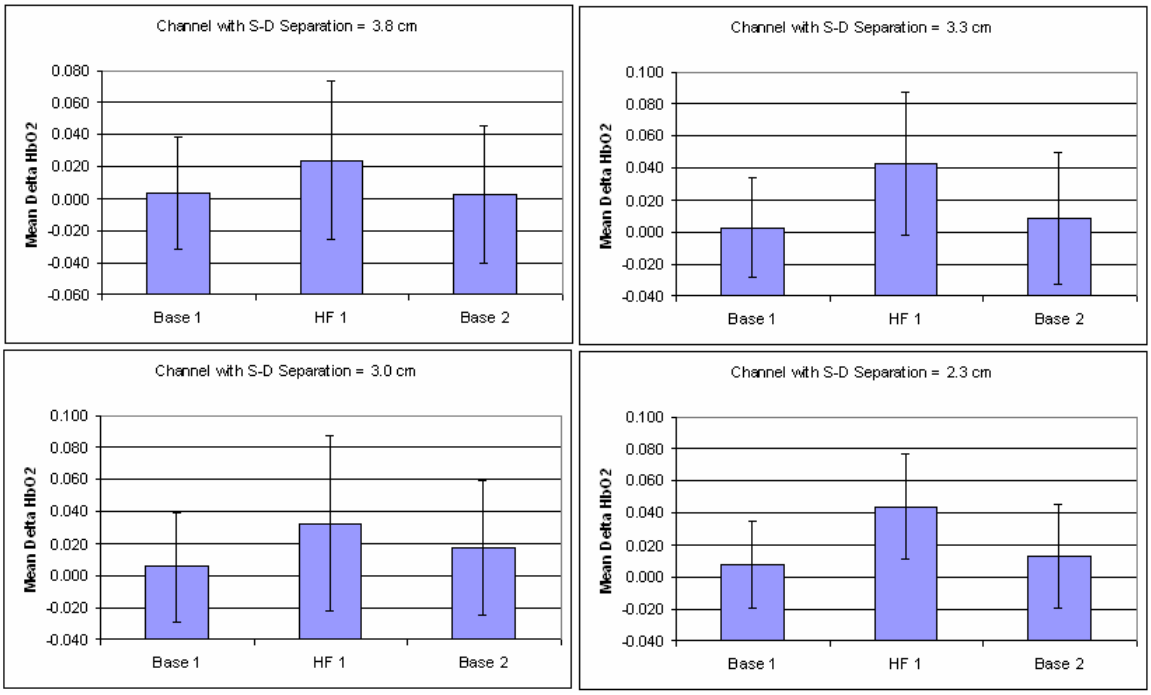

Figure 5.14 Plot of Mean ΔHbO2 for all detectors for Subject 3

Figure 5.13, 5.14 shows the plot of mean ΔHbt and ΔHbO2, for the four detectors, for Subject 1. The error bars shown is the standard deviation for each region of interest. All the detectors follow similar characteristics as seen in Figures 5.13 to 5.14. During the period when the subject experiences a hot flash event, as reported by the subject, there is an increase in the local blood volume (both ΔHbt and ΔHbO2), followed by a gradual decay toward the baseline. This phenomenon is also in accordance with the changes in skin conductance as seen in Figure 5.12.

Furthermore, student T-test was done to verify that there was a significant difference between the average baseline readings and the average hot flash event readings of ΔHbt and ΔHbO2 for all the channels, respectively. The results of the T-test indicate that there is a significant difference between the baseline reading and the hot flash readings of the respective channels.

5.4 Conclusion

In this chapter, the capability of our LCC – NIRS system to detect hot flashes was studied. The studies proved that the system was able to detect changes in local blood volume during a hot flash event. This system has the potential to be developed further for the detection of hot flashes.

Through this study, the major concern for this system was the amount of noise picked up by it. So, further improvements have to be made in the circuitry of the system for it to be used as a clinical means. The system, if made portable and ambulatory, would be a great tool for the detection of hot flashes. For this application, we would preferably like to have the probe to be made as a single channel probe for the easy placement on the subject's sternum. Thus the probe could be made in different configurations to target different areas of the human body.

CHAPTER 6

SUMMARY AND FUTURE SCOPE

6.1 Conclusion

For my thesis research, I have focused on developing a multi-channel, multi-separation probe for the LCC – NIRS system developed earlier in our lab. As part of my thesis, I have also explored two possible applications of the LCC – NIRS system. The project consisted of three sections: 1) developing a multi-channel, multi-separation probe with source-detector separations of 3.8cm, 3.3 cm, 3.0 cm, and 2.3 cm. Then the newly built probe along with LCC - NIRS system was tested using laboratory phantom, and the results are satisfactory, showing correct functionality of the system. 2) One possible application of the LCC – NIRS system was explored by me with several human subjects, targeting on detection of hot flashes in menopausal women. The results are positive showing the feasibility to use the LCC - NIRS system for hot flash identification and monitoring. I conclude that the probe developed with the LCC – NIRS system can be used to detect hemodynamic changes occurring during hot flashes in the sternal area. 3) Another possible application of the LCC – NIRS system, as a screening tool for the detection of sleep apnea, was explored by me with 4 subjects using the breath holding protocol. The results of the study proved fruitful that the system was able to detect changes between the baseline and the breath hold periods. For the breath holding protocol, hemodynamic changes observed using the probe developed were similar to the

standard LEDI system. The conclusion is that the probe developed by me along with the LCC – NIRS system may have a potential as a screening tool for sleep apnea detection.

6.2 Future Scope

A prototype of a low-cost, compact, multi-channel, multi-separation, LED-based, continuous-wave, near infrared system was developed. After testing, it was concluded that the system works well to show hemodynamic changes during the standard blood-tissue phantom study and also for human subject measurements. However, since it is the first prototype, there are certain improvements that can be done on the system to make it more compact and ready to use in ambulatory conditions. The suggestions for the future work are as follows:

1. The probe could be made in different configurations to target different areas of the human body.
2. Based on the application requirements, the decision on the number of channels can be decided upon, and the circuitry can be changed.
3. A professionally shielded cable from the probe to the data acquisition card would reduce the pick up of electrical noise.
4. The circuit could be made more compact by combining the control board and the probe by building a PCB board and using circuit mount devices. By having a Printed Circuit Board (PCB) built, the effects of noise would also be greatly reduced as the control circuitry and the probe can be incorporated as a single unit.

5. The bulky power supply could be eliminated, and a smaller power supply could be used.
6. The system could be made more ambulatory in nature by making the system as a wireless device.

When all the above features are incorporated, it will make the system more compact and also will be able to detect many kinds of hemodynamic changes in most parts of the human body. Moreover, as the implementation of these changes is feasible, it would further provide more applications for which the system could be used.

APPENDIX A

MATLAB CODES

Code for Data analysis for both hot flash and breath holding protocols

```
% This is a procedure for calculating NIR data.
% Before you can use it, you need to specify:
% filename in the load command: e.g., 'subject1.dat'
% marker locations in time(sec): e.g., if you want first marker at 60 sec,
% then specify marker1=60;
clc;
clear all;
close all;
marker1=491;
marker2=535;
% extinction coefficients
eHbO_850 = 2.6694;
eHbO_730 = 1.0089;
eHb_730 = 2.9993;
eHb_850 = 1.8096;
A = load('C:\Documents and Settings\Pradeep\My Documents\LabVIEW
Data\subject1.lvm');
A=A(1:end,:);
baselinesample = 30;

A730 = A(:,[2 3 4 5]);
[d,c] = butter(4,0.02);
A730 = filtfilt(d,c,A730);

A850 = A(:,[6 7 8 9]);
[d,c] = butter(4,0.02);
A850 = filtfilt(d,c,A850);

A805 = A(:,[10 11 12 13]);
% A805 = A805*1000;
time = A(:,1)/(5);

%Plot Raw Data
figure;
subplot(2,2,1);
plot(time, A730);
v = axis;
hold on; line([time(marker1*5) time(marker1*5)], [v(3) v(4)]);
line([time(marker2*5) time(marker2*5)], [v(3) v(4)]); hold off;
xlabel('Time, (min)');
ylabel('Raw Data');
title('Raw Data for 730nm');
```

```
legend('Ch1','Ch2','Ch3','Ch4',-1);

subplot(2,2,2);
% figure;
plot(time, A850);
v = axis;
hold on; line([time(marker1*5) time(marker1*5)], [v(3) v(4)]);
line([time(marker2*5) time(marker2*5)], [v(3) v(4)]); hold off;
xlabel('Time, (seconds)');
ylabel('Raw Data');
title('Raw Data for 850nm');
legend('Ch1','Ch2','Ch3','Ch4',-1);

subplot(2,2,3);
% figure;
plot(time, A805);
v = axis;
hold on; line([time(marker1*5) time(marker1*5)], [v(3) v(4)]);
line([time(marker2*5) time(marker2*5)], [v(3) v(4)]); hold off;
xlabel('Time, (seconds)');
ylabel('Raw Data');
title('Raw Data for 805nm');
legend('Ch1','Ch2','Ch3','Ch4',-1);

subplot(2,2,4);
plot(time, A850 + A730);
v = axis;
hold on; line([time(marker1*5) time(marker1*5)], [v(3) v(4)]);
line([time(marker2*5) time(marker2*5)], [v(3) v(4)]); hold off;
xlabel('Time, (seconds)');
ylabel('Raw Data');
title('Raw Data for 730nm + 850nm');
legend('Ch1','Ch2','Ch3','Ch4',-1);

%Calculate HB & HBO2 & BV
baseline730 = mean(A730(1:baselinesample,:));
baseline850 = mean(A850(1:baselinesample,:));
compare730 = ones(size(A730,1),1)*baseline730./A730;
compare850 = ones(size(A850,1),1)*baseline850./A850;
HB = 1*(-0.5497*log10(compare850) + 1.04579*log10(compare730));
HBO2 = 1*(-0.81386*log10(compare730) + 1.430549*log10(compare850));
BV = HB + HBO2;

%  figure ;
```

```
for i=1:4
   figure ;
%    subplot(2,2,i);
   plot(time, HB(:, i), 'r');
   hold on;plot(time, HBO2(:,i), 'b');
   plot(time, BV(:, i), '--black'); hold off;
   v = axis;
   hold on;
   line([time(marker1*5) time(marker1*5)], [v(3) v(4)]);
   line([time(marker2*5) time(marker2*5)], [v(3) v(4)]);
   hold off;
   xlabel('Time (Seconds)');
   ylabel('delta Concentration');
   cntr = num2str (i);
   X = [3.8 3.3 3.0 2.3];
   cntr1= num2str (X(i));
    Mystring = strcat ('HB, HBO2, and HB Total for Channel',cntr,' at SD separation ',' = ',
cntr1, 'cm');
   title(Mystring);
   legend('HB', 'HBO2', 'HBt',-1);
   Mypath = strcat('c:/data/detect/',cntr);
% saveas(gcf,Mypath,'fig');
end
```

APPENDIX B

IRB APPROVAL FORMS

THE UNIVERSITY OF TEXAS AT ARLINGTON

SCHOOL OF NURSING

Date: May 2, 2005

To: Dr. Hanli Liu
Biomedical Engineering
19138

Re: **Protocol 05.349** *A Study of Cerebral Hemodynamics during Breath Holding Task Using Near Infrared Spectroscopy*

The Institutional Review Board (IRB) has reviewed and approved this research protocol under an expedited review in accordance with Title 45 CFR 46.110. Continuing review is scheduled for one year from the above approval date.

The Office for Human Research Protections (OHRP) requires you to submit annual and final reports for review and approval by the IRB. The annual report must be on file with the IRB before the anniversary date of your initial approval. OHRP does not allow for a grace period on the continual review requirement. If the annual report is not received by the IRB by the anniversary date, the IRB will be forced to terminate the approval of your protocol and if your study is federally funded, the IRB will have to report the termination to OHRP as required by Title 45 CFR 46.103(b) 5.

If you require modifications to this proposal in the method of use of human subjects in this study, change in the Principal Investigator (PI) or Co- Investigator(s), or any change in the subject pool, you are required to obtain prior approval from the IRB before implementing the modification as required by Title 45 CFR 46.103(b) 4iii.

The IRB approved consent form that is stamped by the IRB with the expiration date of the approval must be used for all informed consent procedures on all human subjects in this study. The signed consent forms must be under lock and key on UTA campus for the duration of the study plus three years. These consent forms are subject to inspection during this time period by the IRB, Research Compliance staff and / or federal agents.

All investigators listed in this protocol must have documented Human Subjects Involved in Research (Tier II) training on file with the Office of Research Compliance. Please call the Office of Research Compliance if you have not taken the training course within the last year.

If you have any questions related to this research or to the IRB, you may contact me at (817) 272-4840 or the Office of Research Compliance at (817) 272-3723.

Sincerely,

Dr. Jennifer Gray

Dr. Jennifer Gray
Assistant Professor
IRB Chair

BOX 19407 411 S NEDDERMAN DR ARLINGTON, TEXAS 76019-0407 T 817.272.2776 F 817.272.5006 http://www.uta.edu/nursing

IRB Protocol #
FUNDED GRANT #
CONTRACT #

Office . Research Compliance
Phone (817) 272-3723
Fax (817) 303-1111

THE UNIVERSITY OF TEXAS AT ARLINGTON

SUBJECT CONSENT FORM

I have been asked to participate as a subject in the research project entitled *A study of cerebral Hemodynamics during breath holding task using near infrared spectroscopy*
under the direction of *Dr. Hanli Liu*

PURPOSE OF THE STUDY

I understand that the purpose of this study is to *Measure oxygen levels in the brain during specific task*

PROCEDURES

There is an experiment designed to study the effects of breath holding on the cerebral heamodynamics. A non-invasive probe will be attached to the forehead of the subject. The subject will be asked to hold the breath after a baseline (2 minute) and release the breath after the maximum possible hold. There will be a wait period (5 minutes) to obtain the baseline again. The experiment lasts for less than 10 minutes.

NUMBER OF SUBJECTS PARTICIPATING

Approximately 20 healthy subjects will participate in the experiment.

The approximate number of subjects involved in the study should be stated in the consent form.

RISKS OF PARTICIPATION

I understand that the potential risks from participation in the study are *none*

BENEFITS TO THE SUBJECT

I understand that I will not benefit from my participation in the research project.

ALTERNATIVE TREATMENT

The alternative is not to participate in the study

APR 2 9 2005

APPROVED BY THE UTA-IRB
The IRB approval for this consent document will expire on

APR 2 8 2006

IRB Protocol #_____
FUNDED GRANT #_____
CONTRACT #_____

Office of Research Compliance
Phone (817) 272-3723
Fax (817) 303-1111

I voluntarily agree to participate as a subject in the above named project. I understand that I will be given a copy of the consent form I have signed.

Date _____ Signature of Subject _____

Using language that is understandable and appropriate, I have discussed this project and the items listed above with the subject and/or his/her authorized representatives.

Date _____ Signature of Principal Investigator _____

APR 2 9 2005

APPROVED BY THE UTA-IRB
The IRB approval for this consent document will expire on

APR 2 8 2006

IRB Protocol #_____
FUNDED GRANT #_____
CONTRACT #_____

Office of Research Compliance
Phone (817) 272-3723
Fax (817) 303-1111

ADDENDUM TO SAMPLE SUBJECT CONSENT

OTHER INSTRUCTIONS AND CLAUSES THAT MAY BE REQUIRED

PREGNANT SUBJECTS:

A. In protocols where risk is minimal and there is no medical reason to exclude pregnant subjects, then no particular reference to pregnancy is required.

B. In protocols which pose a medical risk to the pregnant subject or to the fetus there should be a sentence in the consent form which states the following:

Pregnant subjects are to be excluded from this research project. In order to qualify for inclusion in this study, all women of childbearing potential must have a negative pregnancy test.

C. In the recruitment notice for protocols in which there is a medical risk to the pregnant subject or to the fetus the following statement should be included:

Pregnant subjects are to be excluded from this research project. In order to qualify for inclusion in this study, all women of childbearing potential must have a negative pregnancy test.

REQUIREMENTS FOR ASSENT/CONSENT BY CHILDREN:

1. The assent to participate in a research protocol should be obtained in all children at and above the age of seven (7).

2. When children are being asked to assent to participate in research, the following statement should be included in the consent form as standard clause #10:

My child has had the risks and benefits of the research explained to him/her in language that he/she can understand and has agreed to participate in this research.

3. Children with at least a cognitive age of an average 2nd grader or about seven years of age should sign on an "assent" line as the "subject" of the research. This is in addition to his/her parents signature(s) on the "authorized third party" line.

4. The issue of advocates for children who need them will be determined on a case by case basis.

5. If the research procedure holds the possibility of direct benefit that is important to the well-being of the child or the capability of the child is so limited that assent/consent is not possible, the IRB can choose to waive the requirement of assent/consent.

INFORMED CONSENT PROCESS

APR 2 9 2005

The principal investigator has the difficult task of explaining the proposed activity to a potential

APPROVED BY THE UTA-IF
The IRB approval for this cons
document will expire on

APR 2 8 2006

Office of Research Compliance
Phone (817) 272-3723
Fax (817) 303-1111

subject in enough detail and in appropriate language so as to assure that the potential subject fully understands what he/she is consenting to and that the consent is an educated one.

The Institutional Review Board has the equally difficult task of determining whether or not the consent procedure proposed by the principal investigator adequately assures legally informed consent of the subject. To assist the principal investigator in better preparing subject consents, the following statements may be helpful.

The subject consent form must identify the activity to be conducted, name(s) and the phone number of the individual(s) who are to conduct the activity and state the purpose of the activity. It must describe any procedures that are deemed to be experimental in nature and indicate the risks attendant thereto. It must also refer to any prior experience gained in human use or state that no prior human use has occurred and indicate the experience that has been acquired in animal studies.

A statement should be made about expected or potential reactions resulting from all procedures to be performed that are not deemed to be experimental. The benefits, if any, that could accrue from the activity should be described and a statement made as to whether the benefit would accrue to the individual subject or to society in general. Alternative procedures that could be used in lieu of the experimental procedures must be described. An offer to answer any inquiries concerning the procedure should be made in writing. The subject should also be informed in writing that he/she may discontinue participation in the activity at any time without prejudice to the subject.

It is important that the terminology used in the subject consent form be such that it is understandable and relevant to the average lay person rather than the investigator.

It is the responsibility of the Institutional Review Board to be satisfied that the subject consent will be obtained without undue inducement or any element of force, fraud, deceit, duress or other forms of constraint or coercion.

Each subject should be given a copy of the consent form he or she has signed.

If personal data is to be acquired from surveys, questionnaires or medical records it is necessary to inform the subject of the criteria used by which he or she was selected to be a subject, describe the purpose for which the data is being collected, indicate any benefits to be gained by the subject's participation in the activity, and state what risks (physical, psychological, or social) or possible detrimental effects that may accrue to the subject. The investigator should describe the plan by which the confidentiality of personal data will be assured. Documents, discs, tabs, coded keys, etc., which contain personal data that may place the subject at risk of losing confidentiality should be stored in a locked area with access to that area limited only to the investigator or other authorized personnel. The investigator should also develop a plan for the destruction of such personal data at an appropriate time and in a specified manner.

When an activity proposes to use normal subjects, the subject should be informed that no benefit will be derived from his/her participation. The inducements offered to a normal subject should be consistent with the degree of remuneration and shall not unduly influence the subject to participate in the activity.

If randomization (by chance) is used to select a subject population, the subject must be so

APR 2 9 2005

APPROVED BY THE UTA-IRB
The IRB approval for this consent document will expire on

APR 2 8 2006

Office of Research Compliance
Phone (817) 272-3723
Fax (817) 303-1111

informed.

The investigator should incorporate into the subject consent the length of time required for participation in the activity, whether this is continuous or intermittent, any requirement for follow-up examinations or studies and whether or not there will be limitations or constraints on the physical activities of the subject after the activity is completed.

If monitoring procedures are required during the activity, the type, number and frequency of such procedures should be explained and the risks or discomforts of each should be described. If the performance of such procedures will incur additional expense to the subject, he/she should be so informed.

If the research subject or his/her insurance company will be expected to pay for any expenses incurred by participation in the research protocol, this must be explained in the consent form.

The signed consent forms must be kept under lock and key for a minimum of 3 years after the conclusion of the research. For research funded by the federal government, the signed informed consent forms for each participant must be kept for 3 years (or more depending on the funding agency) after final close-out by the Office Grant and Contract Services at UTA. All signed consent forms will be subject to quarterly monitoring by the Institutional Review Board.

APR 2 9 2005

APPROVED BY THE UTA-IRB
The IRB approval for this consent document will expire on

APR 2 8 2006

APPENDIX C

CORRELATION BETWEEN HEMODYNAMIC PARAMETERS AND SKIN CONDUCTANCE

CORRELATION BETWEEN HEMODYNAMIC PARAMETERS AND SKIN CONDUCTANCE

This Appendix deals with the relationship between the hemodynamic parameters changes in peripheral blood flow and the skin conductance changes. This study was conducted, to test whether there was a relationship between blood flow and skin conductance during normal activity. This study was done to prove that the skin conductance changes were not entirely affected by the local blood flow.

C.1 Lab Measurement Protocol Using LCC – NIRS and Biolog Skin Conductance Level meter (Biolog SCL - 3991x/1)

1. The human subjects taking the experiment were notified about the detailed procedures.
2. The probe, designed for the LCC-NIRS system, was placed on one of the forearms of the human subject. The room was dark during the experiment to reduce interference due to ambient light. The Biolog skin conductance electrodes, i.e., two Ag/AgCl disposable electrodes were placed on the palm of the same arm.
3. The electrodes were connected to the ambulatory Biolog Skin Conductance Level meter via an input assembly with two standard male snaps at the lead ends.
4. The subject was instructed to sit on a chair with his/her arms stretched out and the fingers pointing towards the ground for about 2 minutes, when the baseline was obtained.
5. The subject was asked to raise his/her arm above his/her head in one swift motion and hold the position for 2 minutes, which was considered the stimulus period.
6. The subject was asked to return back to the original position, again in one swift motion, and then hold the position for a period of about 2 minutes.

The study was done for 5 subjects, all male; all of them were volunteer students from UTA.

C.2 Results for Lab Measurement

Five subjects were recruited for the simultaneous study measuring the hemodynamic parameters and the skin conductance. The results obtained from the study are as follows, for:

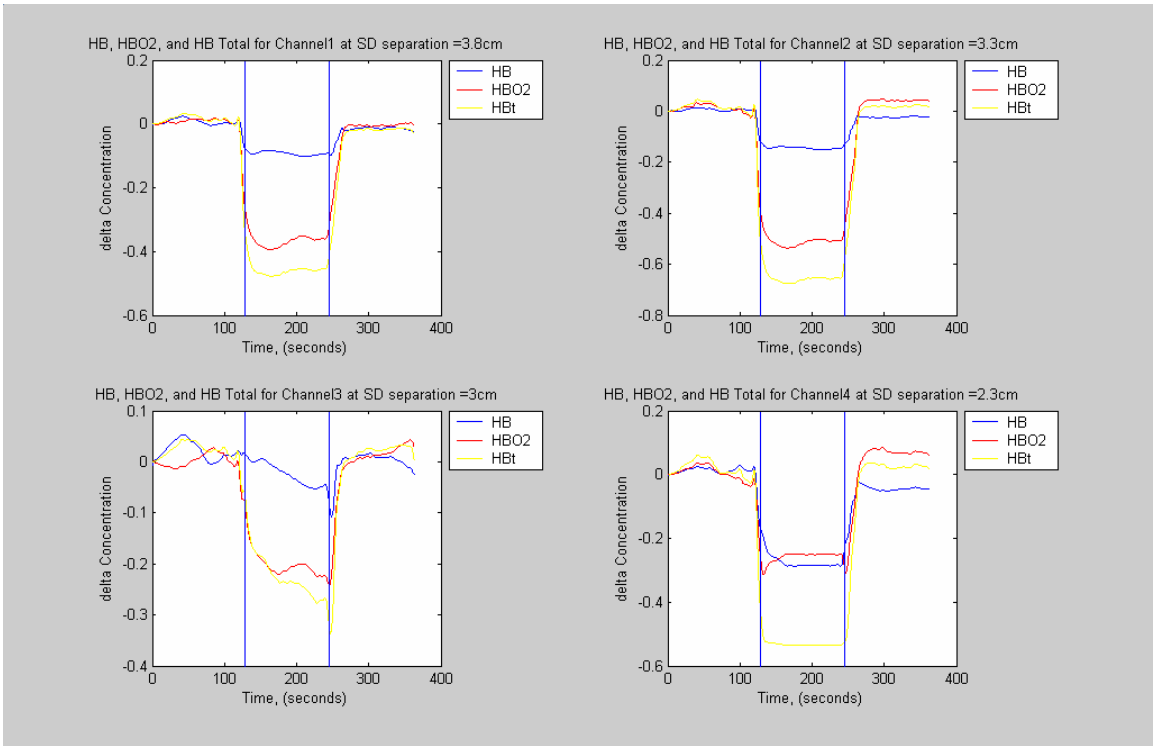

Figure C-1 Subject 1 – Plot of Hb, HbO2 and Hbt for all detectors

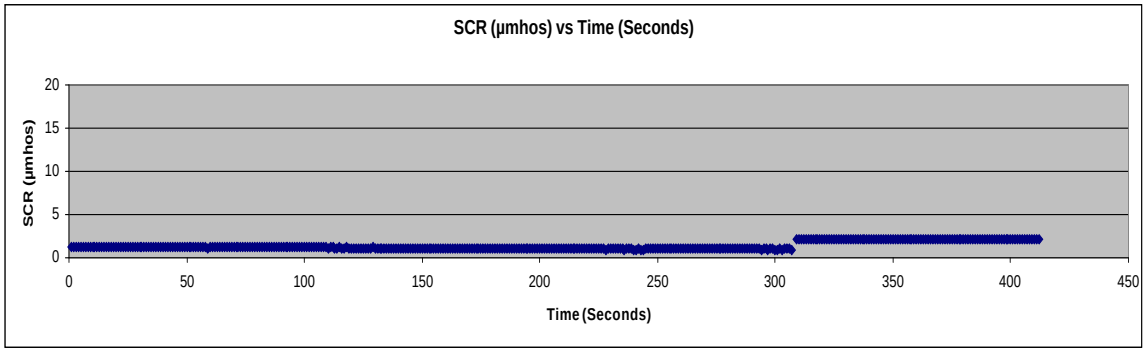

Figure C-2 Subject 1 - Plot of the Skin Conductance (µmho) vs. Time (seconds)

Figure C.1 shows the filtered plot of Hb, HbO2 and Hbt, for all channels for the first subject. The noisy signal was filtered using a fourth order Butterworth low pass filter, with a cut-off frequency of 0.05 Hz. The same filter was applied to all the other channels too. The first marker represents the time when the subject lifted his/her arm above the head in one swift motion. The second marker represents the time when subject lowers the arm. As seen in the figure, HbO2 and Hbt started to decrease sharply as the arm was raised. Hb decreased by a little margin during the same period. The margin of decrease of Hb was very irregular when compared within the detectors. This phenomenon can be attributed to lesser blood flow towards the end fingers as the resistance to flow of blood is increased due to gravity. Thus the LCC – NIRS was able to detect changes in blood flow accurately. As seen from figure C.2, the skin conductance did not change by much for the whole measurement.

Figures C.3 to C.10 shows the filtered plots of Hb, HbO2 and Hbt and the skin conductance level for the rest of the subjects. All of them recorded similar changes in Hb, HbO2 and Hbt. But the skin conductance data varied randomly for each subject.

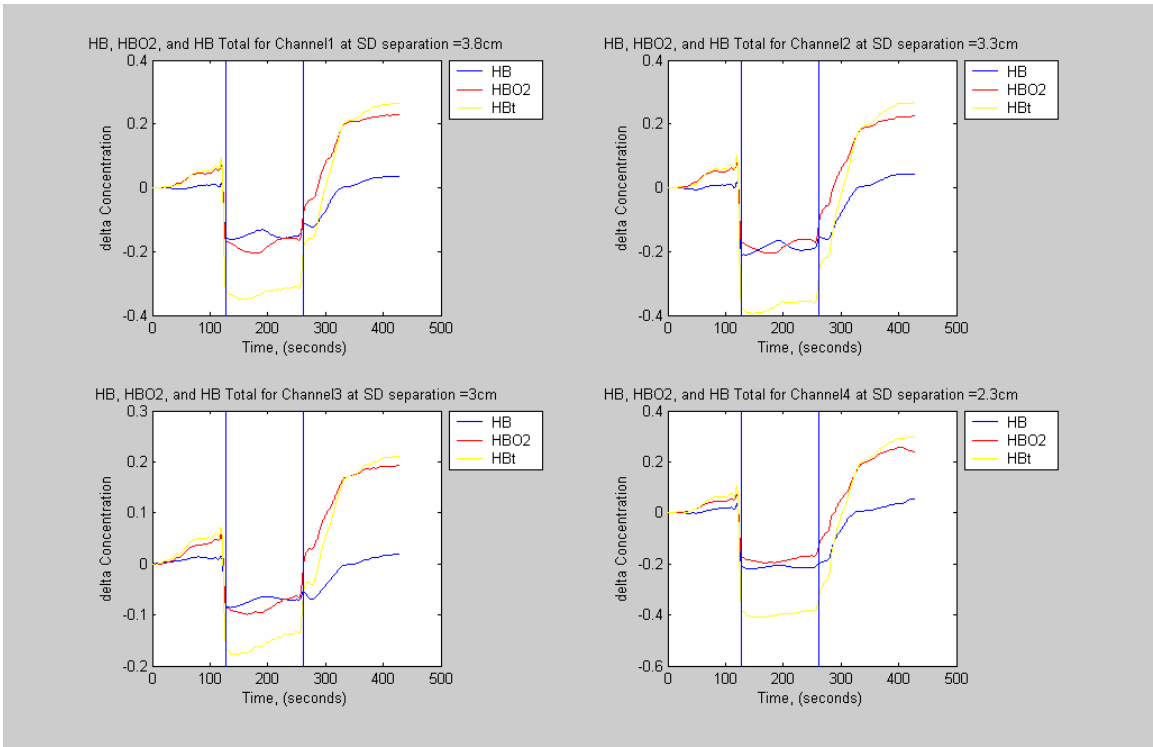

Figure C-3 Subject 2 – Plot of Hb, HbO2 and Hbt for all detectors

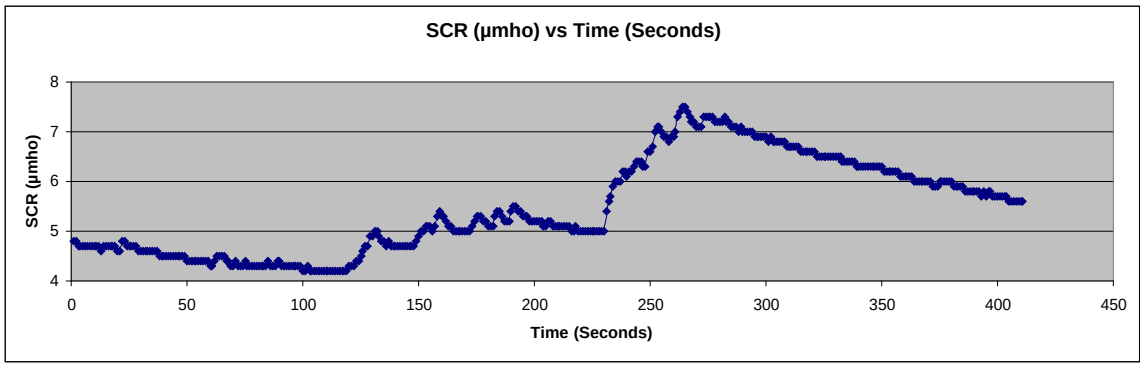

Figure C-4 Subject 2 - Plot of the Skin Conductance (µmho) vs. Time (seconds)

As seen in Figure C.3, all the three parameters show similar changes as shown by the first subject. Figure C.4 shows a sudden increase in the SCR data. This can be attributed to the motion artifact due to the clenching of the fist by the subject during this period. The NIRS probe was placed on the upper part of the forearm, near the elbow region; therefore the probe was not affected due to the motion of the palm.

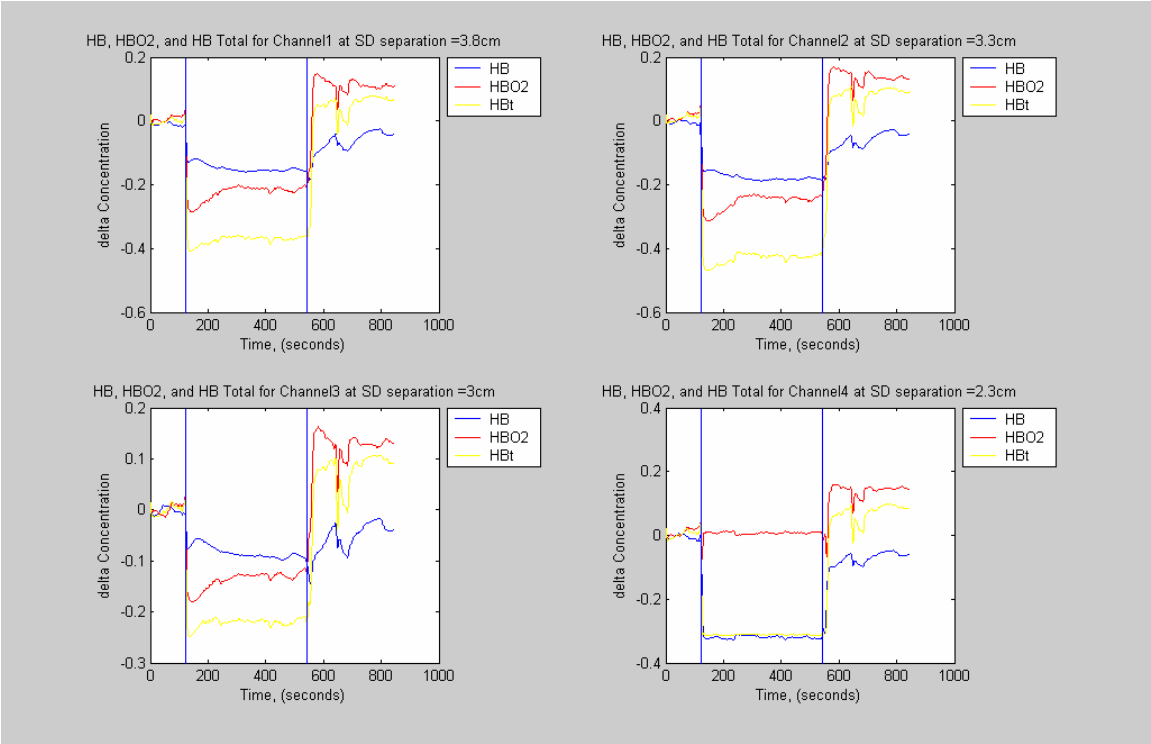

Figure C-5 Subject 3 – Plot of Hb, HbO2 and Hbt for all detectors

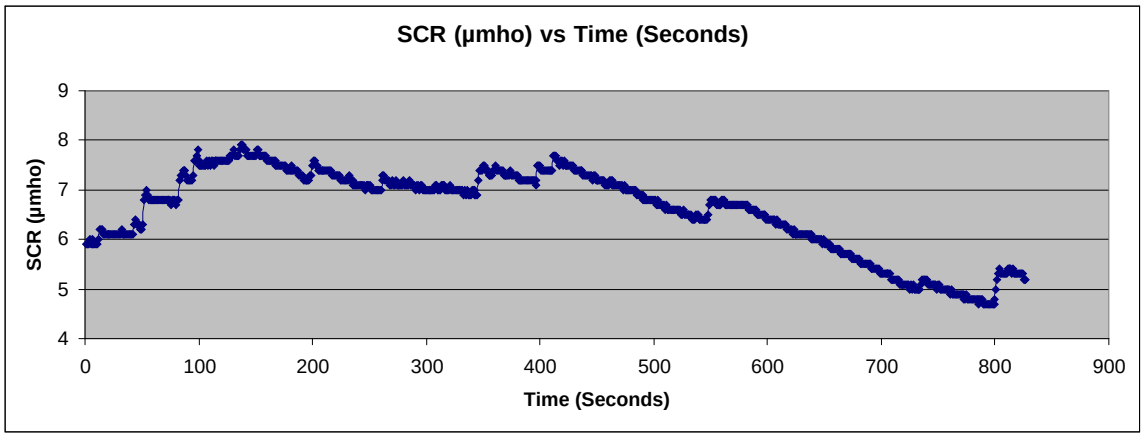

Figure C-6 Subject 3 - Plot of the Skin Conductance (µmho) vs. Time (seconds)

Figure C.5 shows the filtered plots of Hb, HbO2 and Hbt for subject 3. The stimulation period for this subject was for 420 seconds (7 minutes). Therefore, due to the length of the stimulation period, the subjects hand moved during the second baseline period. The irregularities picked up by all the channels of the NIRS probe correspond to

the above mentioned motion artifact. The SCR data, as seen in figure C.6, dropped by about 1 micro mho during this period to settles at around 5 micro mhos.

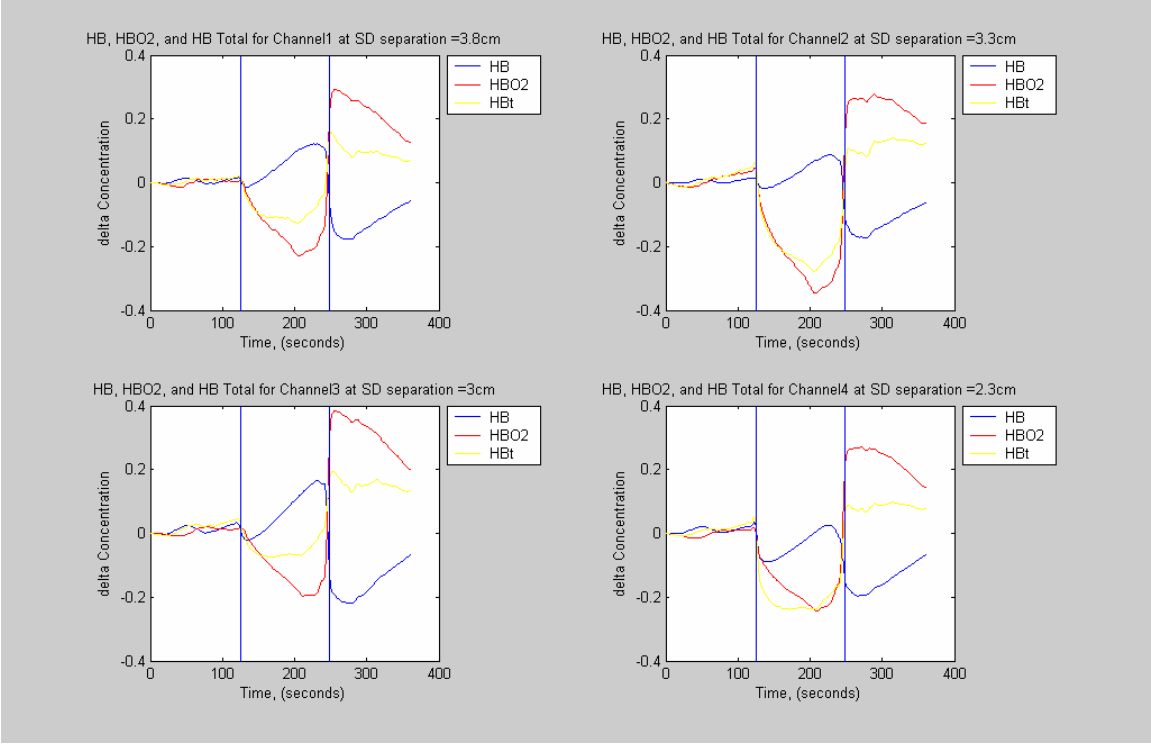

Figure C-7 Subject 4 – Plot of Hb, HbO2 and Hbt for all detectors

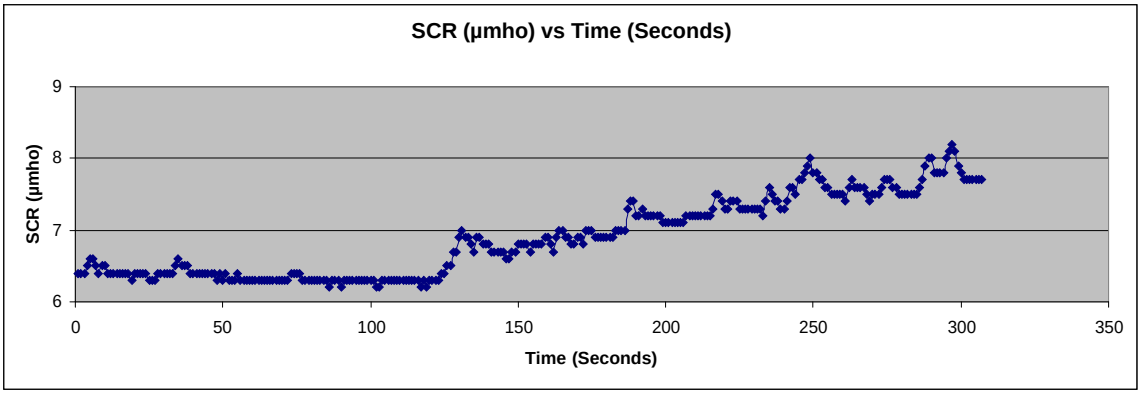

Figure C-8 Subject 4 - Plot of the Skin Conductance (µmho) vs. Time (seconds)

Figure C.7 shows the filtered plots of Hb, HbO2 and Hbt for subject 4. The slow reduction in the HbO_2 and Hbt can be attributed to the slow speed of the arm movement.

The other interesting feature to be noted in this subject's data is that the Hb is first reducing for a few seconds and then starts to increase during the stimulation period. The skin conductance also starts to increase during the start of the stimulation period and still increases during the second baseline period.

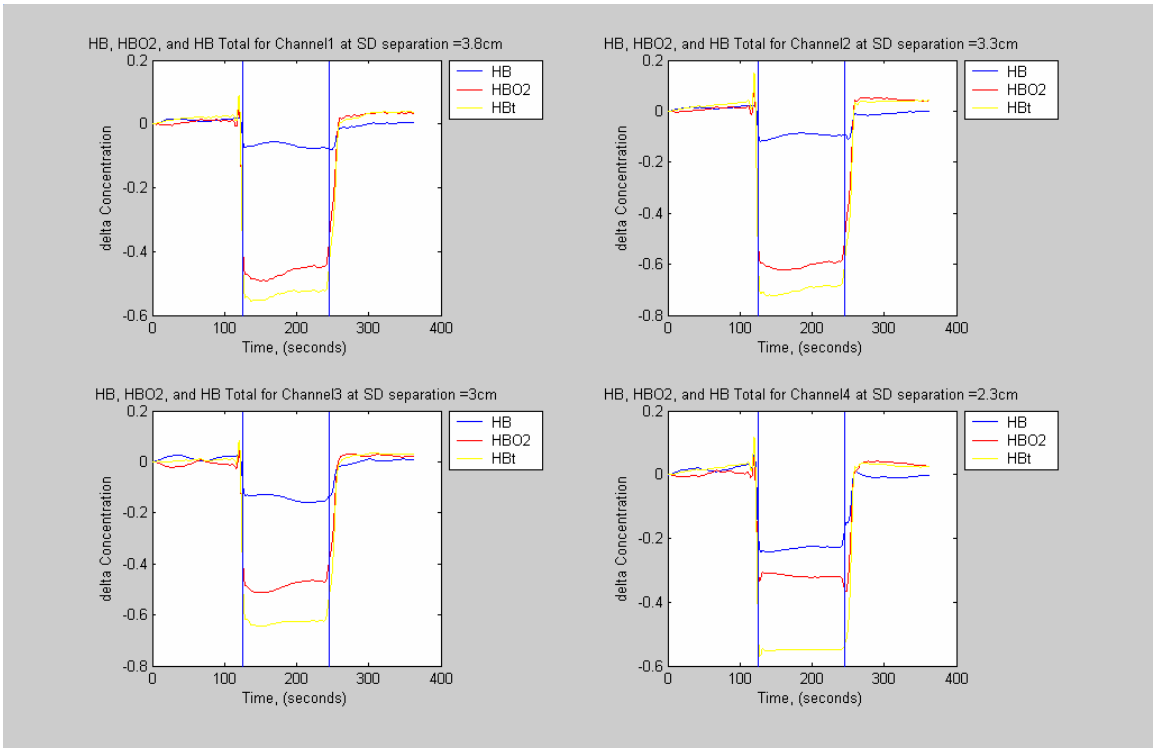

Figure C-9 Subject 5 – Plot of Hb, HbO2 and Hbt for all detectors

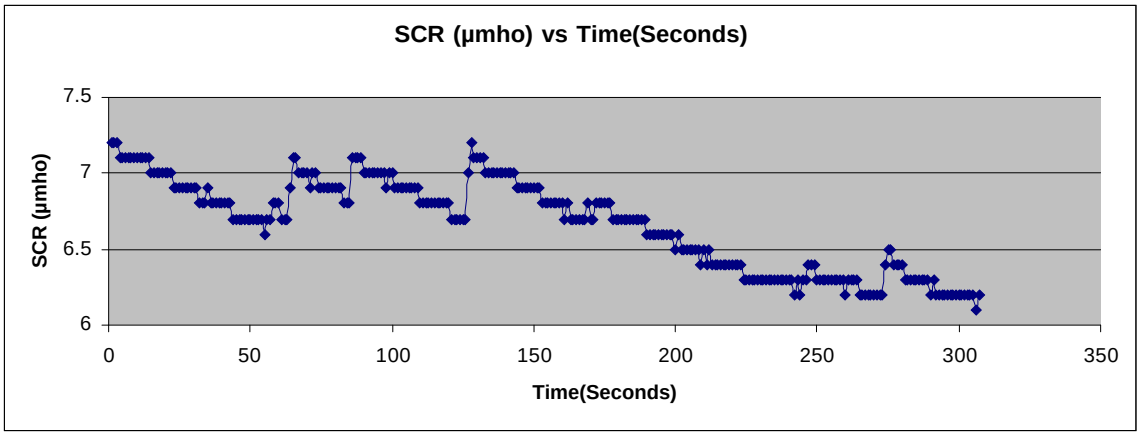

Figure C-10 Subject 5 - Plot of the Skin Conductance (µmho) vs. Time (seconds)

Figure C.9 shows the filtered plots of Hb, HbO2 and Hbt for subject 5. All the three parameters start to go down instantly during the start of the stimulus period. The margin of change for Hb was comparatively lower than the other two parameters. The peak at the beginning of the stimulus period was due to the jerking motion of the arm while lifting it up above the head. The speed of movement of the arm was very fast. The SCR started to drop at the start of the stimulus period and still continued to drop thereafter until the end.

The hemodynamic change due to the change in blood flow was recorded by the NIRS system. There was no correlation between the changes in blood flow and the skin conductance as shown by the data got from the study undertaken above.

REFERENCES

1. Ryer, A., Light Measurement Handbook (pp. 1-8). International Light.
2. Website of Hitachi Medical, "http://www.hitachi-medical.co.jp/info/opte/Kaisetsu-1.html".
3. Website of Near Infrared Spectroscopic Analytical Method, "http://konarc.naro.affrc.go.jp/sakukai/jouseki/ad07-e.html".
4. Heinko, J.K., Nissila, I.T., Somersalo, E., Kajava, T.T., and Katila, T.E. (2000), "Medical near-infrared imaging"
5. Franceschini, M.A., Fantini, S., Toronov, V., Fillaci, M.E., Gratton, E. (2000), "Cerebral Hemodynamics Measured by Near-Infrared Spectroscopy at Rest & During Motor Activation", Optical Society of America, pp- 73-80.
6. Elwell, C & Hebden, J. Website of Biomedical Optics Research Laboratory at University College of London, "http://www.medphys.ucl.ac.uk/research/borl/research/NIR_topics/nirs.htm".
7. Florian E. W. Schmidt, "Development of a Time-Resolved Optical Tomography System for Neonatal Brain Imaging", Ph.D. Thesis, University College London (1999).
8. Yodh, G.A., Boas D.A. (2003). Functional Imaging with Diffusing Light. Biomedical Photonics Handbook, CRC Press LLC.
9. Hebden, J &

10. Arridge, S. Website of Biomedical Optics Research Laboratory at University College of London, "http://www.medphys.ucl.ac.uk/research/borl/research/NIR_topics/imaging_exp.htm".
11. Fishkin, J.B., Gratton, E.(1993), "Propagation of photon-density waves in strongly scattering media containing an absorbing semi-infinite plane bounded by a straight edge.", Optical Society of America 10, 1: 127-140
12. Gu, Y., Mason, R., Liu, H.(2005), "Estimated fraction of tumor vascular blood contents sampled by near infrared spectroscopy and ^{19}F magnetic resonance spectroscopy", Optics Express, Vol. 13, No. 5, pp. 1724-1733.
13. Liu, H., Y. Song, K. L. Worden, X. Jiang, A. Constantinescu & R. P. Mason (2000). "Non Invasive Investigation of blood oxygenation dynamics of tumors by near-infrared spectroscopy." Applied Optics 39: 5231-5243
14. Casavola, C., Paunescu, L.A., Fantini, S., Gratton, E. (July, 2000). "Blood flow and oxygen consumption with near-infrared spectroscopy and venous occlusion: spatial maps and the effect of time and pressure of inflation." Journal of Biomedical Optics 5(3), 269–276.
14. LEDI Manual, NIM inc., Philadelphia, PA.
15. Sharma, V. – "Near Infrared Spectroscopy: A Study of Cerebral Hemodynamics during Breath holding and Development of a System for Hotflash Measurement", M.S. Thesis, University of Texas at Arlington (August 2005).
16. Li, Rose, "Assessing and Improving Measure of Hot Flashes," Summary of NIH Workshop (Feb 2004). Rose Li and Associates, Inc.

17. Ranga, R., “An In Vitro Hemodynamic Phantom Model For Near Infrared Spectroscopy”, M.S. Thesis, University of Texas at Arlington (May 2005).
18. Product Information, VST – Platinum Silicone Elastomer, VST-50, Factor II, Inc., Lakeside, AZ
19. Luo, Q., Zeng, S., Chance, B., Nioka, S. (2002), “Monitoring of Brain Activity with Near-Infrared Spectroscopy” Handbook of biomedical diagnostics 8: 455-486.
20. Cerussi, A.E., Tromberg, B.J. (2003), “Photon Migration Spectroscopy Frequency-Domain Techniques” Biomedical Photonics Handbook 22.
21. Butler, R. N., “Recent advances in the OSAHS, Sleep, Health and Aging” ILC Workshop Report: 1-28
22. Caples, S.M., Gami, A.S., Somers, V.K. (2005), “Obstructive Sleep Apnea” Annals of Internal Medicine 142:187-197.
23. Kastrup, A., Kruger, G., Neumann, T., & Moseley E.M. (2001). “Assessment of cerebrovascular reactivity with functional magnetic resonance imaging: comparison of CO2 and breath holding.” Magnetic Resonance Imaging **19**: 13-20.
24. Fox, S.I. (1999). Cardiac Output, Blood Flow and Blood Pressure. Human Physiology, McGraw-Hill.
25. Carpenter, J. S., Monahan, P. O., Azzouz, F., “Accuracy of Subjective Hot Flush Reports Compared With Continuous Sternal Skin Conductance Monitoring,” American College of Obstetricians and Gynecologists, Vol. 104, No.6 1322-1326, December 2004.

26. Kronenberg, F., “Menopausal hot flashes: Randomness or rhythmicity,” Chaos Vol. 1, No.3, 271-278, (1991).
27. Stearns, V., Ullmer, L., Lopez, J. F., Smith, Y., Isaacs, C., Hayes, D.F., “Hot flushes,” The Lancet, Vol. 360,1851-18561, December 7,2002.(URL address://http://www.thelancet.com)
28. Kronenberg, F., “Hot Flashes: Epidemology and Phsyiology,” Ann N Y Acad Sci. 180: 312-16 (1990).
29. Li, Rose, “Assessing and Improving Measure of Hot Flashes,” Summary of NIH Workshop (Feb 2004). Rose Li and Associates, Inc.
30. Kronenberg, F., “Hot Flashes: Phenomenology, Quality of Life and Search for Treatment Options,” Experimental Gerontology, Vol. 29, Nos. 3/4 ,pp. 319-336, (1994).
31. Ratka, A. (2005) Menopausal hot flashes and development of cognitive impairment. In: Estrogen and Hormone Therpay in Postmenopausal Women, Ann N Y Acad Sci, 1052: 11-26. Ed. Meharvan Singh, URL : “www.annalsnyas.org”.
32. Miller, H. G., Maria, R., “Measuring Hot Flashes: Summary of National Institute of Health workshop,” Mayo Clin Proc, Vol. 79, 777-781, (2004).
33. “http://www.bio-medical.com”, Bio-Medical Instruments Inc., Warrren, MI.
34. 3991x/1- SCL Extended Memory BioLog "Hot Flash Monitor" and DPS Support Software 3991x System Firmware 1.2, Release Notes & Instructions (2003), UFI, Morro Bay, CA.

35. Dormire, S.L., Carpenter, J.S., “An alternative to Unibase/glycol as an effective nonhydrating electrolyte medium for the measurement of electrodermal activity”, Vol. 39, pp. 423-426, (2002).

BIOGRAPHICAL INFORMATION

Pradheep Raman was born on September 28, 1981 in Tamil Nadu, India. He received his Bachelor of Engineering Degree in Electrical and Communication Engineering from Madras University, India in May 2003. In fall 2003 he started his graduate studies in Biomedical Engineering from Joint Program of Biomedical Engineering at the University of Texas at Arlington and University of Texas Southwestern Medical Center at Dallas, completing it by fall 2005. He has worked extensively on Near Infrared Spectroscopy. His future interests include Biomedical Optics, Image Processing and Electro-medical Instrumentation.